STRUCTURE AND PROPERTIES OF AN AMORPHOUS FERROMAGNETIC ALLOY

Thesis by

Stephen Chung-Hsiung Lin

In Partial Fulfillment of the Requirements

For the Degree of

Doctor of Philosophy

California Institute of California

Pasadena, California

1968

(Submitted May 20, 1968)

ACKNOWLEDGEMENTS

The author wishes to express his gratitude to Professor Pol Duwez for his direction and encouragement throughout this work. He would also like to thank Professors F. S. Buffington and C. J. Pings for their helpful discussions and suggestions. Acknowledgement is due to the U. S. Atomic Energy Commision for their financial support.

ABSTRACT

The structure and the electrical and magnetic properties of an amorphous alloy containing approximately 80 at.% iron, 13 at.% phosphorus and 7 at.% carbon ($Fe_{80}Fe_{13}C_7$) obtained by rapid quenching from the liquid state have been studied. Transmission electron diffraction data confirm the amorphous nature of this alloy. An analysis of the radial distribution function obtained from X-ray diffraction data indicates that the number of nearest neighbors is approximately seven, at a distance of 2.6A. The structure of the alloy can be related to that of silicate glasses and is based on a random arrangement of trigonal prisms of Fe_2P and Fe_3C types in which the iron atoms have an average ligancy of seven. Electrical resistance measurements show that the alloys are metallic. A minimum in the electrical resistivity vs. temperature curve is observed between $10^{o}K$ to $50^{o}K$ depending on the specimen, and the temperature at which the minimum occurs is related to the degree of local ordering. The Fe-P-C amorphous alloys are ferromagnetic. The Curie temperature measured by the induction method and by Mössbauer spectroscopy is $315^{o}C$. The field dependence of the magneto-resistance at temperatures from liquid helium to room temperature is similar to that found in crystalline iron. The ordinary Hall coefficient is approximately 10^{-11} volt-cm/amp-G. The spontaneous Hall coefficient is about 0.6×10^{-9} volt-cm/amp-G and is practically independent of temperature from liquid helium temperature up to $300^{o}C$.

TABLE OF CONTENTS

LIST OF FIGURES

LIST OF FIGURES continued

LIST OF FIGURES continued

LIST OF TABLES

I. INTRODUCTION

It is generally recognized that ordinary silicate glass is a typical example of an amorphous solid. Glass is also defined as a supercooled liquid which differs from ordinary liquids only in its physical properties, but not in its atomic arrangement. This atomic arrangement may extend over a small number of atoms, but does not repeat itself in three directions in space like in a crystal. Thus, the amorphous state may be very similar to the liquid state, except that the atoms are frozen in fixed positions. In the field of glass, a more or less arbitrary line of demarcation between liquid and solid state is related to a viscosity of about 10^{15} poises (cgs units). At that point, there is no noticeable change in the atomic arrangement in the structure.

In recent years amorphous metallic thin films have been produced by high vacuum vapor-deposition method.[1,2,3] Most of these are stable only at low temperature and many of them are too thin to be considered as three-dimensional solid. A recently developed technique[4,5] by which liquid alloys can be quenched at a rate of 10^6 ^{o}C/sec or higher has led to the retention of amorphous structures stable above room temperature. Such amorphous structures have been found in gold-silicon[6], gold-lead[7], palladium-silicon[8,9] and tellurium-base alloys with germanium, gallium and indium.[10] By using the same technique, an amorphous phase was obtained in $Fe_{80}P_{13}C_7$ alloys[11] and a study of the structure and properties of these alloys is the subject of the present investigation.

II. EXPERIMENTAL PROCEDURE

A. Preparation of Alloys

The alloys were prepared by powder metallurgy techniques. The iron powder was less than 40 microns in size and 99.9% purity. The phosphorus was chemically pure red phosphorus powder and the carbon was obtained by filing spectroscopic grade graphite electrodes. The powders were accurately weighed, mixed and pressed in a rectangular steel die 1" x 3/8" x 1/4" at a maximum pressure of 50,000 lb/in^2. The compacts were then sealed in evacuated fused silica capsules. In sintering alloys containing such large amounts of phosphorus it is necessary to follow a temperature-time schedule such that sufficient time is allowed for the phosphorus to react with iron and form one of the stable iron phosphides, in this case Fe_2P. A typical heating cycle was as follows: slow heating up to 580°C in about 70 hours; maintain 580°C (10°C below the melting point of phosphorus) for about 40 hours; increase temperature to 600°C (above the melting point of phosphorus) and maintain this temperature for 40 hours; slow heating to 900°C and maintain this temperature for 40 hours. The structure of the compacts after this sintering treatment was found to consist of three phases; namely, Fe (saturated with C), Fe_3P and Fe_3C. Although the ternary phase diagram Fe-P-C is not accurately known, (see Appendix I) it is probable that these three phases represent the equilibrium structure of the alloy at 900°C.

The sintered alloys were rapidly quenched from the liquid state by the "Piston and Anvil" technique described in Ref. 5. In this technique a small quantity of alloy is melted in a fused quartz "crucible" and a liquid droplet is caught between two plates made of copper. The temperature of the liquid alloy before quenching was approximately 1200°C. Although the alloy is not kept in the liquid state for more than 20 to 30 seconds, losses of phosphorus by evaporation are unavoidable, and the chemical composition of the quenched foils is likely to be different from that of the initial alloy. After the quenching conditions were standardized, it was possible to obtain reproducible results in the composition of the quenched foils. These were chemically analyzed by both wet chemistry and electron-microprobe analysis. The average chemical analysis in at.% of as many as twenty foils studied in this investigation was 79.9 $\pm$ 1% Fe, 13.0 $\pm$ 1% P and 7.0 $\pm$ 0.5% C. The foils were in average 2 cm in diameter and 40 to 50 micron thick.

As explained in Ref. 5 the methods of rapid cooling from the liquid state have not reached a sufficient degree of refinement to insure that every quenched foil has been subjected to the same rate of cooling, and hence the structure of each foil must be checked before measuring its physical properties. Since in this particular case the quenched foil must be amorphous, the absence of Bragg's diffraction peaks was checked by X-ray diffraction. Preliminary experiments showed that deviation from a typical amorphous pattern first occurs within a

limited range of Bragg angles, within which the broad amorphous band is located. A diffraction pattern of each foil was therefore taken within a range of 2θ angles from 45° to 60°, with Co radiation, and with a slow scanning speed of 0.1°/min. All foils for which a slight deviation from a typical amorphous diffraction band was observed, were rejected. In addition, some of the foils were also checked for lack of crystallinity by transmission electron diffraction. A typical electron diffraction pattern obtained by transmission and with 100 kv is shown in Fig. 1.

B. X-ray Diffraction Technique

The study of the atomic arrangement in the amorphous Fe-P-C alloys requires a very accurate determination of the intensity of the diffraction pattern. As in the case of liquid alloys, it is necessary to use a rather short wave length and monochromatic radiation. The diffractometer used in the present study was a G.E. XRD-5, equipped with a Mo anode tube, a lithium fluoride doubly curved monochromator crystal mounted on the diffracted beam, as shown schematically in Fig. 2. The scintillation counter, the amplifier, pulse discriminator, scaler and timer were all the latest (solid state) models from Hamner. Since a complete scanning of the diffraction pattern of an amorphous alloy may require as long as ten days, the reliability of the diffracted intensity measurements greatly depends on the stability of the intensity of the incident X-ray beam and also on that of the counter and associated

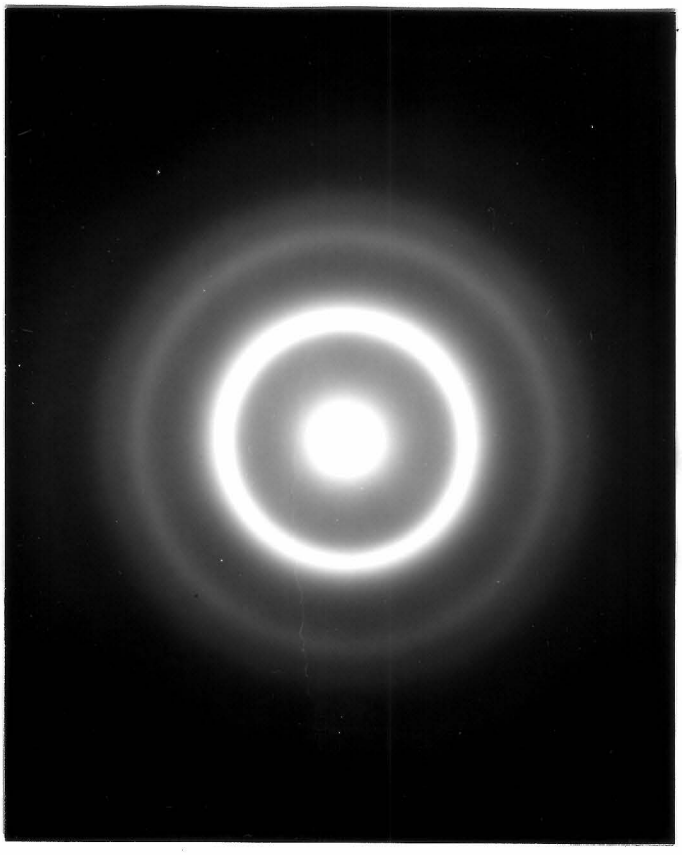

Fig. 1. Transmission electron diffraction of amorphous FePC alloy.

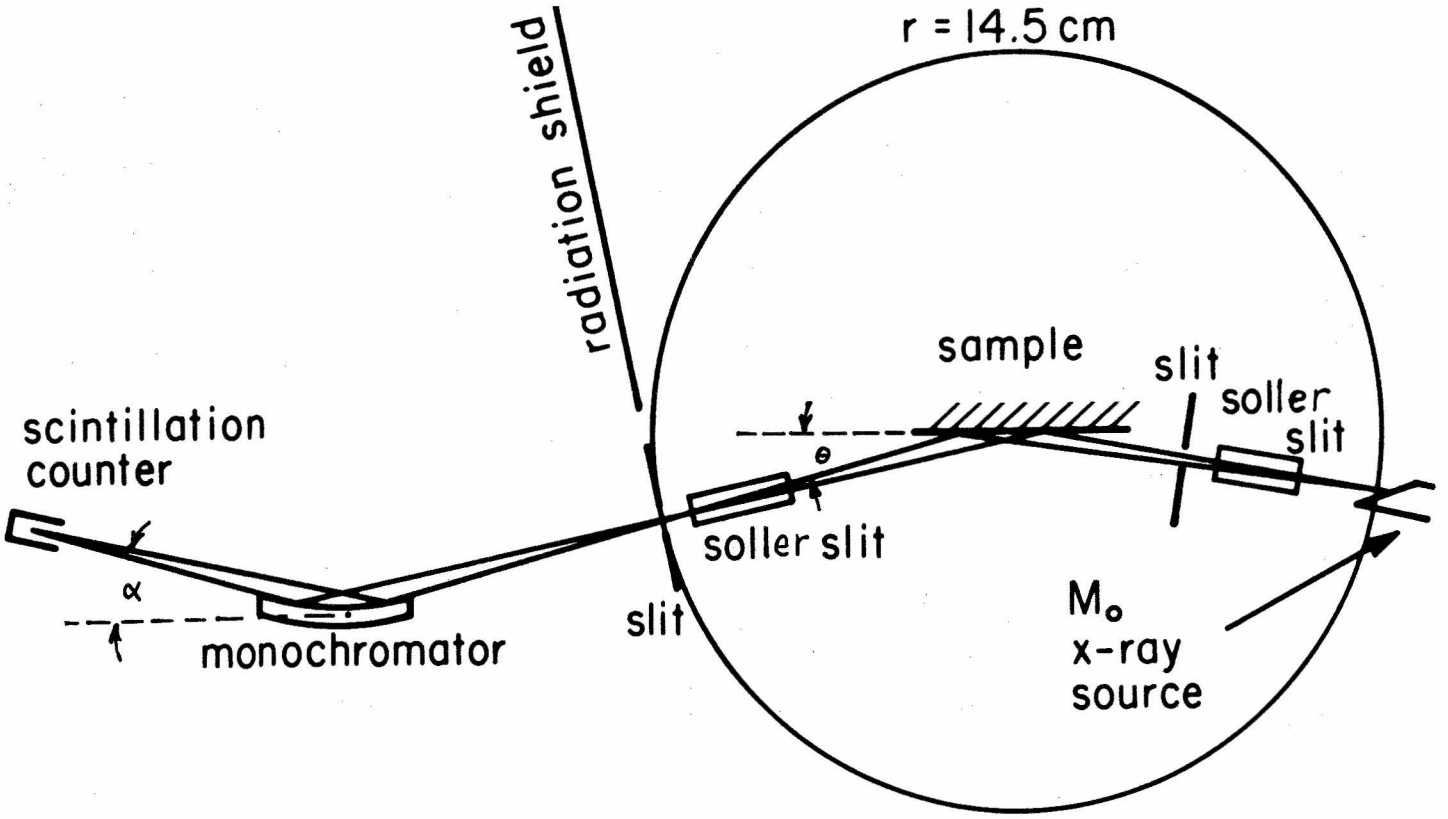

Fig. 2. X-ray diffractometer with crystal monochromator.

electronic equipment. In order to separate these two sources of uncertainty, the long time stability of the recording system was first checked by using a radioactive isotope source. The intensity of this source was chosen at three different levels corresponding approximately to those expected as maximum, minimum and intermediate in the diffraction pattern. The intensities were about 400, 100 and 30 counts per second. These tests were carried out for as long as 120 hours. In all cases, the probable error did not exceed that calculated one for the total number of counts accumulated and no systematic drift with time could be detected. The same experiments were repeated with X-radiation from the Mo anode tube set at 45 kV and 38 mA, with an amorphous FePC specimen. Three levels of intensity were again recorded, and no noticeable either short or long time (up to 100 hours) fluctuations were observed.

The diffraction patterns of amorphous foils were recorded with the diffractometer moving at a given angular rate and the timer - printer combination set for a given time. A complete recording covering a range of 2θ values from 10^{o} to 163^{o} takes about 10 days. At 163^{o}, the value of $S = \frac{4\pi \sin\theta}{\lambda}$ is about 17. Typical scanning conditions are as follows: from 10 to 26^{o} in 2θ, 1^{o} X-ray tube divergent slit, 0.02^{o} in 100 sec, one data point every 0.02^{o}; from 26^{o} to 62^{o} in 2θ, 1^{o} tube slit, 0.02^{o} in 100 sec, one data point every 1000 sec; from 58^{o} to 100^{o} in 2θ, 3^{o} X-ray tube divergent slit, 0.02^{o} in 100 sec, one data point every 1000 sec; from 100^{o} to 163^{o} in 2θ, 0.04^{o} in 100 sec, one data

point every 1000 sec. The range from 58^{o} to 62^{o} in 2θ was scanned with both 1^{o} and 3^{o} divergence slits in order to obtain the intensity ratio so that the two curves could be normalized.

In the X-ray diffractometer technique, the intensity of the diffracted beam must be corrected for absorption. However, this correction becomes independent of the Bragg angle when the diffracting specimen is thicker than a certain value determined by its mass absorption coefficient. In the present case of a FePC alloy, this critical thickness exceeded that of a single foil (approximately 50 microns). In order to avoid the use of an angular dependence of the absorption correction, three or four amorphous foils were glued together (with a very thin layer of Duco cement) on a bakelite substrate. This procedure also helped in obtaining a very flat surface exposed to the incident X-ray beam, which is a very important factor at low Bragg angles.

C. Electrical and Magnetic Measurements

The specimens for electrical resistance measurements were cut out of the foils into rectangular pieces 2.2 x 0.5 cm by electro-discharge machining under oil. Current and potential leads made of a 0.063 inch in diameter nickel wire were spot welded to the specimen (Fig. 2a). The resistance was measured between 4.2 and $1200^{o}K$ and the temperature was measured with a germanium thermometer up to $77^{o}K$ and with a copper-constantan thermocouple between $77^{o}K$ and room temperature. The specimen located in an evacuated fused silica tube, was then transferred to a tube furnace for measurements up to about $1200^{o}K$. In this range, the temperature was measured by a Pt-PtRh thermocouple spot welded to the specimen. The measurements were made by the conventional null technique

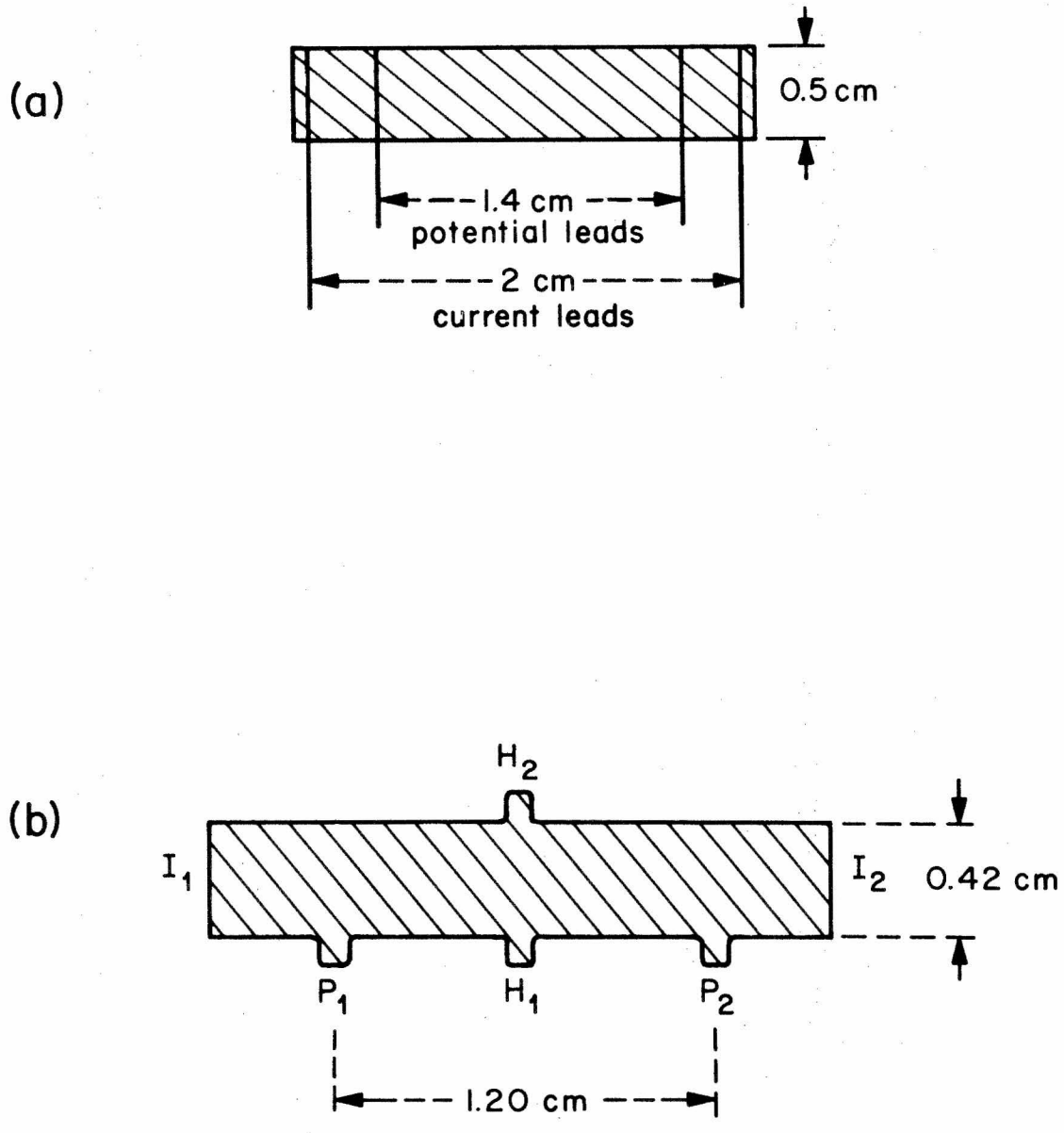

Fig. 3. (a) Sample dimensions for electrical resistance measurements.
(b) Sample dimensions for Hall effect measurements.

with current reversal. No measurable thermoelectric effects were observed by changing the polarity. For the Hall effect, the specimen were shaped as indicated in Fig. 2b and six copper wires were soldered to the specimen with indium solder at points indicated in Fig. 2b in which I_1 and I_2 are for current, P_1 and P_2 for potential and H_1 and H_2 for Hall voltage. Hall coefficients were measured at four temperatures by immersing the specimen in a constant temperature bath. These temperatures were 4.2°K (liquid helium), 77°K (liquid nitrogen), 233°K (freon No. 22) and room temperature. A uniform magnetic field was provided by a 12" Varian magnet and the field, measured with a Varian F-8 flux meter varied from 0 to 9.5 kG. The Hall voltage was measured with a Wenner potentiometer and a nanovoltmeter (Keithley Instrument Co.). Both current and field were reversed in order to minimize misalignment of specimen and thermal effects. For measurements above room temperature the specimen was located in a small furnace within a one inch gap of a 4 inch Varian magnet and the temperature was controlled within $\pm$ 0.5°C.

The spontaneous magnetization of the alloys was measured with a null-coil pendulum magnetometer described in Ref. 12. Because of the high sensitivity of the instrument, only about 2 mg of the amorphous FePC foil was required. Magnetic moments were measured in a temperature range from 1.71°K to room temperature, with fields varying from 4 to 10.7 kG.

The Curie temperature of the alloys was measured by an induction method. The specimen, located in an evacuated fused silica tube, was placed within a heating coil (with D.C. current) and the assembly inserted in an induction coil. The transition from the paramagnetic to the ferromagnetic state was detected by an unbalance of a wheatstone bridge. The apparatus was calibrated by checking the Curie temperature of pure nickel and the estimated uncertainty in transition temperature was within $\pm$ 0.5^{o}C. The Curie temperature was also measured by Mössbauer spectrocopy. The hyperfine field was measured from 4.2^{o}K to 800^{o}K. The amorphous FePC specimen, about 1.5 cm in diameter and 50 micron in thickness was used as an absorber, with a source made of 10 mc of Co^{57} in palladium.

III. EXPERIMENTAL RESULTS

A. X-Ray Diffraction Intensity Curve and Radial Distribution Function

A typical X-ray diffraction curve of an amorphous FePC alloy is shown in Fig. 4. The original curve from which the data were taken was of course drawn with much larger scales and showed many details which are lost in Fig. 4. Before proceeding with the computation of a radial distribution function, the intensity vs. Bragg angle curve must be corrected for background, absorption, polarization and incoherent scattering. The background intensity I_b was 0.7 counts per second.

Since, as explained in section II.B the specimen was quite thick, the absorption correction is independent of the Bragg angle and can be neglected. Assuming that the X-ray beam incident on the specimen is unpolarized its intensity I_o is equally divided between two components $I_{o\perp}$ and $I_{o//}$ respectively perpendicular and parallel to the plane defined by the incident and diffracted beams. The intensity of the scattered beam with the perpendicular component is unchanged; however, that of the parallel component is modified by the factor $\mathrm{Cos}^2 2\theta$.[13] If, as shown in Fig. 2, the scattering angle is 2θ on the sample and 2α on the monochromator, the total final intensity after being diffracted by the sample and the monochromator is

$$I_o' = I_{o\perp} + I_{o//} (\mathrm{Cos}^2 2\theta)(\mathrm{Cos}^2 2\alpha)$$

$$I_o' = \frac{I_o}{2} (1 + \mathrm{Cos}^2 2\theta \ \mathrm{Cos}^2 2\alpha)$$

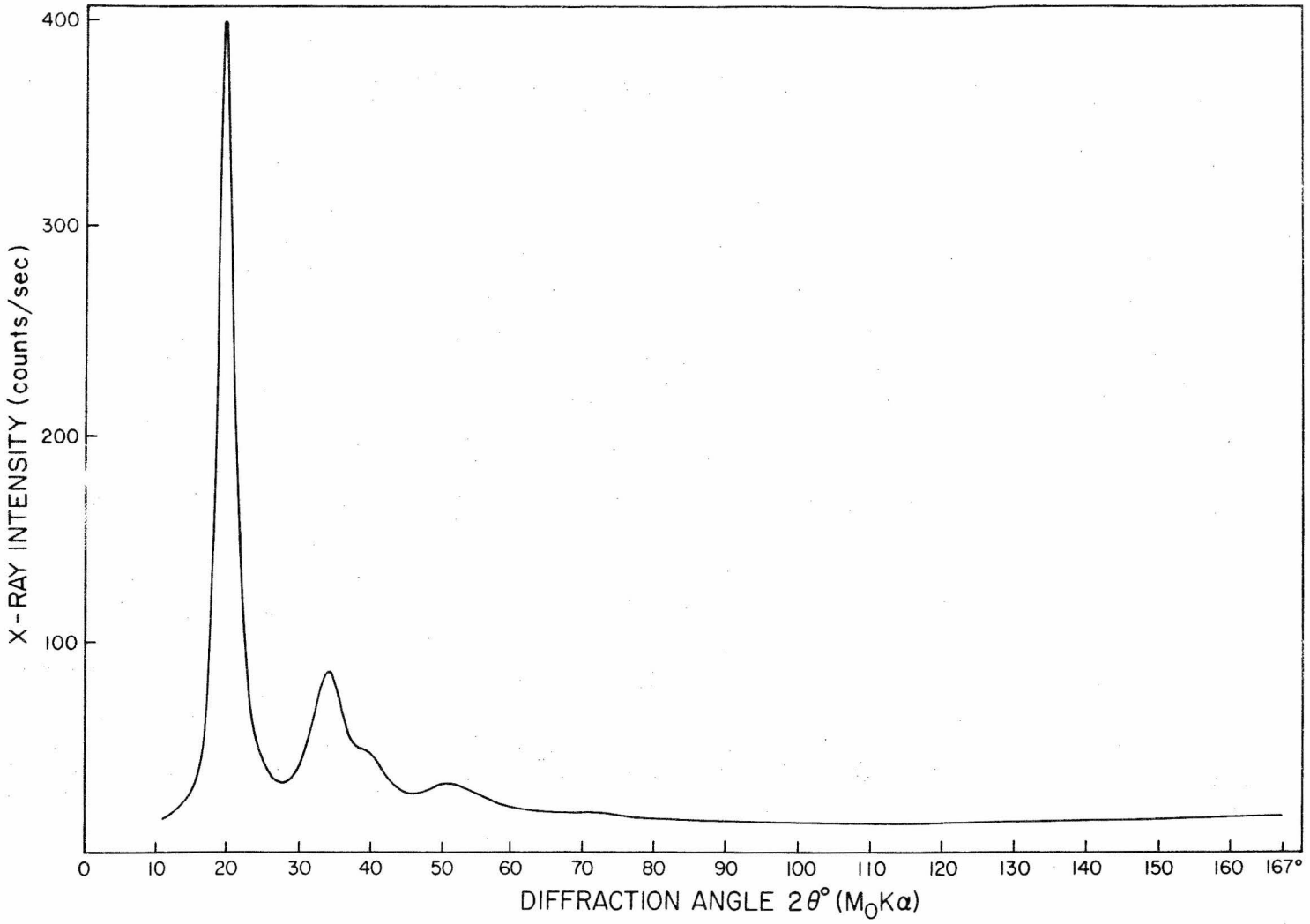

Fig. 4. X-ray diffraction spectrum for amorphous $Fe_{80}P_{13}C_7$.

The reciprocal of the angular dependent part of the expression on the right, $(1 + \text{Cos}^2 2\theta \ \text{Cos}^2 2\alpha)^{-1}$, is the polarization factor for use when a monochromator is located in the diffracted beam.

In the present case, no incoherent scattering correction is necessary since the monochromator is located in the diffracted beam. Hence the corrected intensity, I'' in arbitrary units is given by

$$I'' = (I_{exp} - I_b) \frac{1}{(1+\text{Cos}^2 2\theta \text{Cos}^2 2\alpha)}$$

in which I_{exp} is the measured intensity and I_b is the background intensity.

The next step is to calculate a scaling factor in order to obtain an intensity curve expressed in absolute electron unit. This was done by assuming that the observed intensity at large scattering angles converges to the sum of the squares of the atomic scattering factors in the specimen. The intensity curve vs. $S = \frac{4\pi \text{Sin}\theta}{\lambda}$ so obtained is shown in Fig. 5. The second curve shown on the same figure is the sum of the square of the scattering factors. The scattering factor for each element must be corrected for dispersion. The scattering factor can be expressed as:

$$f = f_o + \Delta f' + i \, \Delta f''$$

$$f^2 = (f_o + \Delta f')^2 + (\Delta f'')^2$$

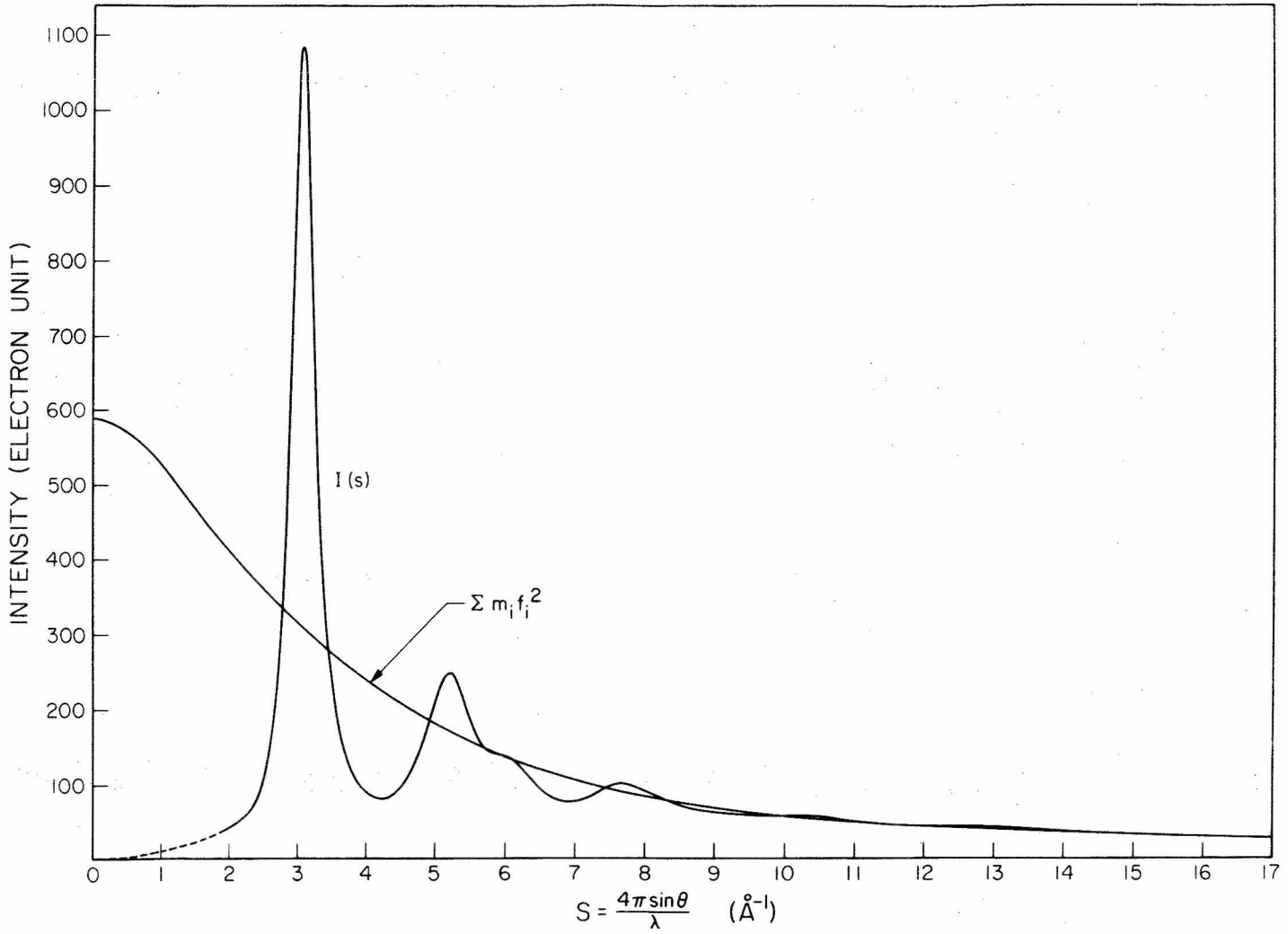

Fig. 5. X-ray diffraction spectrum of amorphous $Fe_{80}P_{13}C_7$ after polarization correction and scaling.

The values for the dispersion correction terms were taken from Cromer[14] and Waber[15] and were: $\Delta f' = 0.37$, $\Delta f'' = 0.92$ for iron; $\Delta f' = 0.11$, $\Delta f'' = 0.12$ for phosphorus; and $\Delta f' = \Delta f'' \approx o$ for carbon.

The next step in calculating the radial distribution function is to perform a Fourier inversion. An approximate solution to the X-ray Fourier inversion for an amorphous polyatomic sample was first provided by Warren, Krutter, and Morningstar[16] who took advantage of the close agreement between reduced scattering factors f/Z (Z being the number of electrons in the scatterer) for atoms of nearly the same atomic number (e.g. vitreous B_2O_3 and SiO_2). Thus the electron scattering factor $f_e = f/Z$ can be adopted and is almost independent of atomic number and the inversion is thus possible. Another point of view concerning polyatomic samples was emphasized by Pings and Washer[17] and Washer and Schomaker.[18] That is, the intensity function can be more explicitly written as a sum of terms characteristic of different kinds of pairs of atoms instead of different kinds of atoms. Since the Fourier transform of a sum of products is a sum of the transforms of these products (linearity of the inversion process), the inversion of the X-ray intensity will be the sum of the distribution functions of different kinds of pairs.

Using the "pair" concept above, Debye's equation can be written as follows. The total amplitude of X-ray scattered coherently is

$$\bar{F} = \sum_{k}^{N} \bar{F}_k$$

where $\bar{F}_k$ is the scattered vector from the k atom and N is total number of atoms.

The intensity becomes

$$F^2 = \bar{F} \cdot \bar{F}^* = \sum_{k=1}^{N} f_k^2 + \sum_{\ell} \sum_{k}' f_\ell f_k \frac{\text{Sin } sr_{\ell k}}{sr_{\ell k}} \qquad (1)$$

Σ' summation exclude self multiplication.

Assuming there are a total of N atoms of first kind N_1, second kind $N_2, \ldots\ldots, p_{th}$ kind N_p, then

$$N = N_1 + N_2 + \ldots\ldots + N_p$$

Equation (1) can be rewritten as

$$F^2 = \sum_{j=1}^{p} N_j f_j^2 + \sum_{j}^{p} N_j f_j \sum_{i}^{p} f_i \int_o^\infty 4\pi r^2 \, n_{ij}(r) \frac{\text{Sin } rs}{rs} \, dr$$

The term $4\pi r^2 \, n_{ij}(r) \, dr$ is the number of i kind of atoms at a distance between r and r + dr from a j kind of atoms. The intensity per atom is

$$I = \frac{F^2}{N} = \sum_{j=1}^{p} m_j f_j^2 + \sum_{j}^{p} m_j f_j \sum_{i}^{p} f_i \int_o^\infty 4\pi r^2 n_{ij}(r) \frac{\text{Sin } rs}{rs} \, dr$$

Set $i(s) = I - \sum_{j}^{p} m_j f_j^2$

Then

$$si(s) = \int_o^\infty \left[\sum_{j}^{p} m_j f_j(s) \sum_{i}^{p} f_i(s)\right] 4\pi r n_{ij}(r) \text{Sin } rs \, dr \qquad (2)$$

In order to do the inversion, it is necessary to separate out the s-dependency in the bracket. The upper limit of the integration is ∞

instead of R(the max. interatomic distance in practice). The reason is that, since R is much greater than the nearest neighbor distance (order of a few $\mathring{A}$), $n_{ij}(r)$ converges very fast to the average atomic density n_o. The intensity due to n_o is found to be concentrated at very small value of s, of the order D^{-1}, D being the linear dimension of an atom. For small values of s the scattering is essentially the same for specimens of non-uniform scattering density. The value of i(s) at low angles is not experimentally measured. Its omission has the consequence that the resulting function represents the difference between the actual distribution function and that corresponding to a uniform, homogeneous density. With $f_e = \frac{\Sigma m_i f_i}{\Sigma m_i Z_i}$ and $K_i = \frac{f_i}{f_e}$ equation (2) becomes

$$4\pi r^2\left[\sum_j^p \sum_i^p m_j K_i K_j n_{ij}(r) - \sum_j^p \sum_i^p m_j K_j K_i m_i n_o\right] = \frac{2r}{\pi}\int_o^\infty \frac{si(s)}{f_e^2(s)} \text{ Sin } rs\, ds$$

$$R_t = \sum_j \sum_i R_{ij} = \sum_j^p \sum_i^p m_j K_i K_j (4\pi r^2 n_{ij}(r)) = n_o\left(\sum_i^p m_i K_i\right)^2 + \frac{2r}{\pi}\int_o^\infty \frac{(si(s)}{f_e^2(s)} \text{ Sin } rs\, ds \quad (3)$$

in which n_o is the average atomic density and $R_{ij} = m_j K_i K_j\ (4\pi r^2 n_{ij}(r))$ = number of electron pairs per atom, each pair consisting of an electron from i kind of atom located at a distance r from an electron from j kind of atom. The value of n_o is detected from the measured density of amorphous FePC (see Appendix II) which is 6.97 ± 0.05 g/cm^3. The iron-iron atom pairs contribute $R_{Fe-Fe} = m_{Fe} K_{Fe}^2\ 4\pi r^2 n_{Fe-Fe}(r)$ electron pairs in the summation on the left hand side of equation (3).

If this term is approximately equal to R_t, then the atomic radial distribution function of Fe-Fe pairs is approximately

$$4\pi r^2 n_{Fe-Fe} = \frac{R_{Fe-Fe}}{2m_{Fe} K_{Fe}^2} \approx \frac{R_t}{2m_{Fe} K_{Fe}^2}$$

In an amorphous FePC sample about 90% of the electron pairs come from Fe-Fe atom pairs, because of the large atomic number of iron compared with phosphorus and carbon.

The radial distribution function resulting from these calculations is shown in Fig. 6. From this function it was found that the first, second, third and fourth nearest neighbors are located at 2.6, 4.3, 5.1 and 6.6 A respectively. The number of nearest neighbors is approximately seven. Data are compared with that of liquid iron[19], vapor-deposited iron[20] and crystalline α-Fe in Table I.

B. Electrical Resistance Measurements

An accurate value of the resistivity of an amorphous FePC alloy is difficult to obtain because of the uncertainties in measuring the dimensions of very small specimens. An approximate value for this resistivity is 180×10^{-6} Ω -cm. This value is slightly higher than that of liquid iron near its melting point which is 139×10^{-6} Ω -cm according to Powell[21] and 110×10^{-6} Ω -cm according to Mokrovskoi and Regel.[22] Since for the purpose of the present study, the temperature dependence of the electrical resistance is more important than the

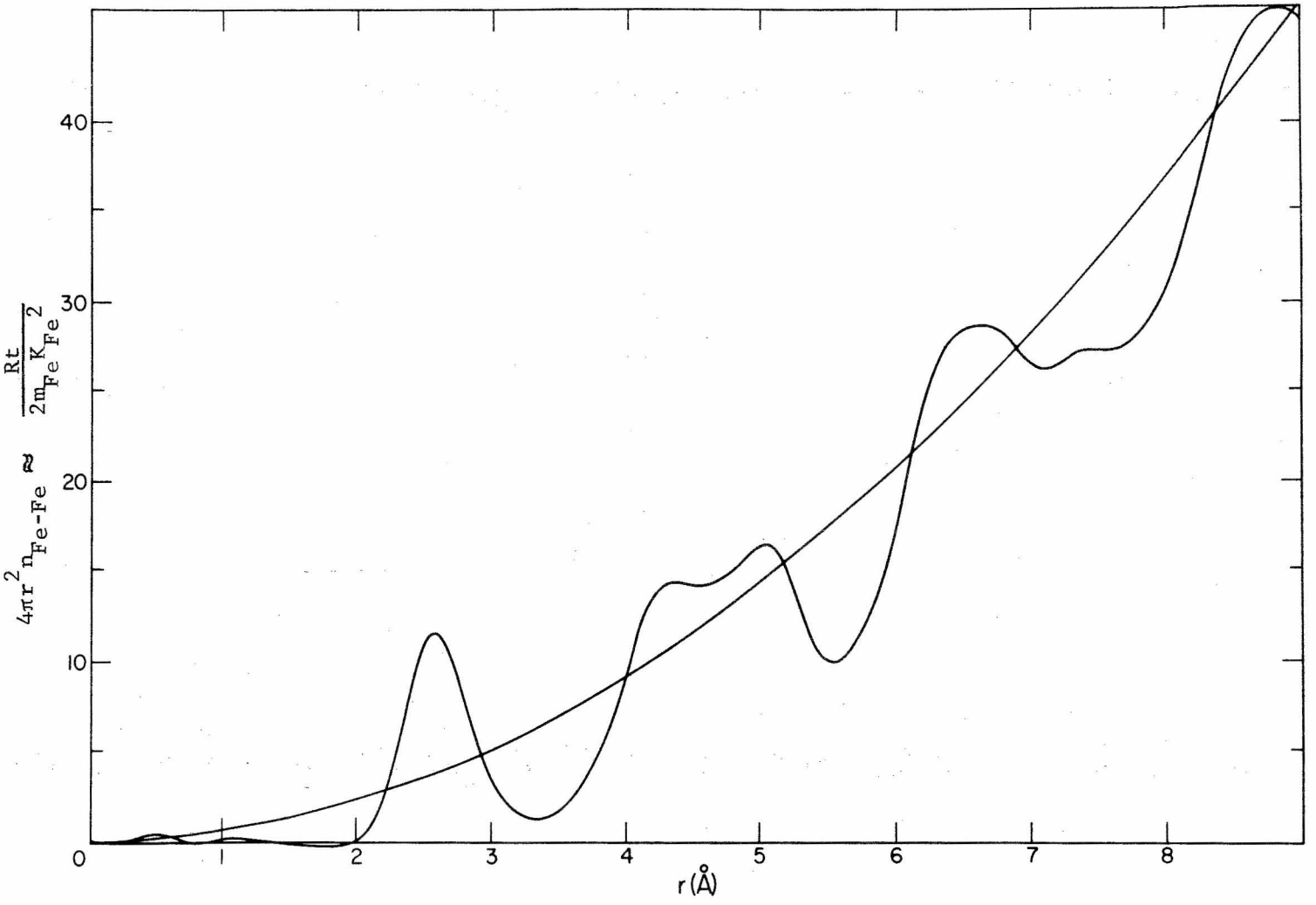

Fig. 6. Atomic radial distribution function of amorphous $Fe_{80}P_{13}C_7$ alloy.

TABLE I

SUMMARY OF THE NUMBER (N_1) AND LOCATIONS (r_n) OF NEAREST NEIGHBORS IN AMORPHOUS FePC ALLOY AND IN LIQUID, AMORPHOUS AND CRYSTALLINE IRON

Sample	Amorphous FePC quenched from liquid state	Liquid Iron[19]	Amorphous Iron[20] vapor-deposited Å	Crystalline Iron
N_1	~ 7	8.4	< 8	8
r_1	2.6Å	2.51	2.6Å	2.48
r_2	4.3Å	4.5	4.5	2.88
r_3				4.08
r_4				4.78

absolute resistivity value, the results will be reported in terms of the ratio of the resistance at any given temperature to that at room temperature ($20^{o}C$). A typical plot of this resistance ratio vs. temperature is shown in Fig. 7. For comparison a curve is also shown for a fully crystallized specimen of the same composition. It is obvious that the resistance of the amorphous alloy is much less sensitive to temperature than that of the crystalline alloy, a fact previously reported in an amorphous Pd-Si alloy also obtained by rapid quenching from the liquid state. In the present case, more than 90% of the room temperature resistance is retained near absolute zero temperature.

In addition, the resistance ratio curve presents a minimum (not clearly shown on Fig. 7, because of the contracted vertical scale) in the vicinity of $20^{o}K$.

As previously explained in section IIA, the method of rapid quenching from the liquid state is not very reproducible and the ultimate quenching rate is not always reached. In this case, it has been found that in foils which are not quenched fast enough, a few dispersed microcrystals are present within an amorphous matrix. These crystals have an effect on the electrical resistance-temperature relationship. To study this effect, about fourteen quenched foils were investigated, and six typical resistance-temperature curves are shown in Fig. 8 in which the vertical scale has been much expanded compared with that in Fig. 7. These curves clearly show that the slope of the resistance-temperature curve at about $100^{o}K$ varies appreciably from specimen to

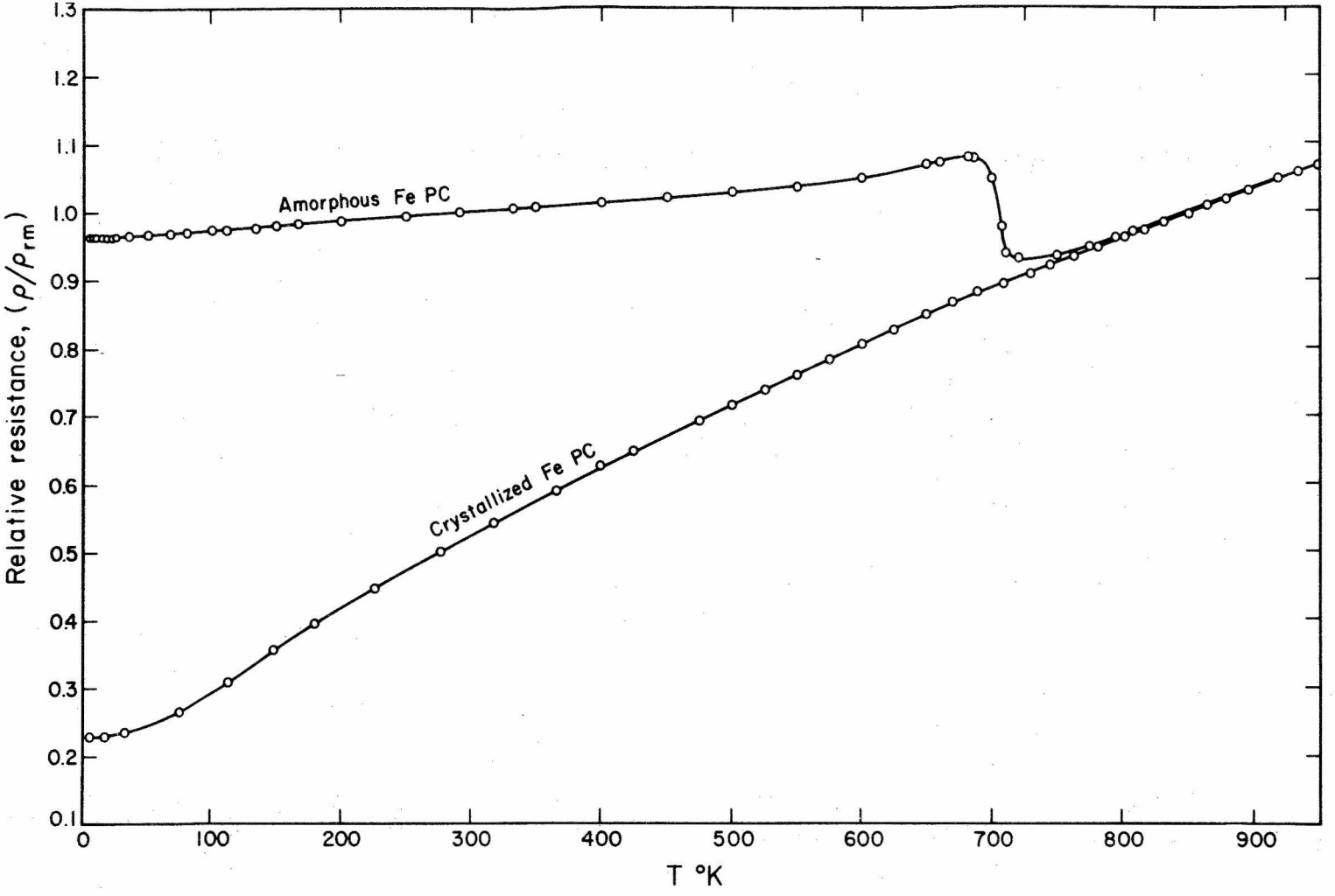

Fig. 7. Relative electrical resistance versus temperature from liquid helium temperature to 950°K for amorphous and crystallized FePC alloy.

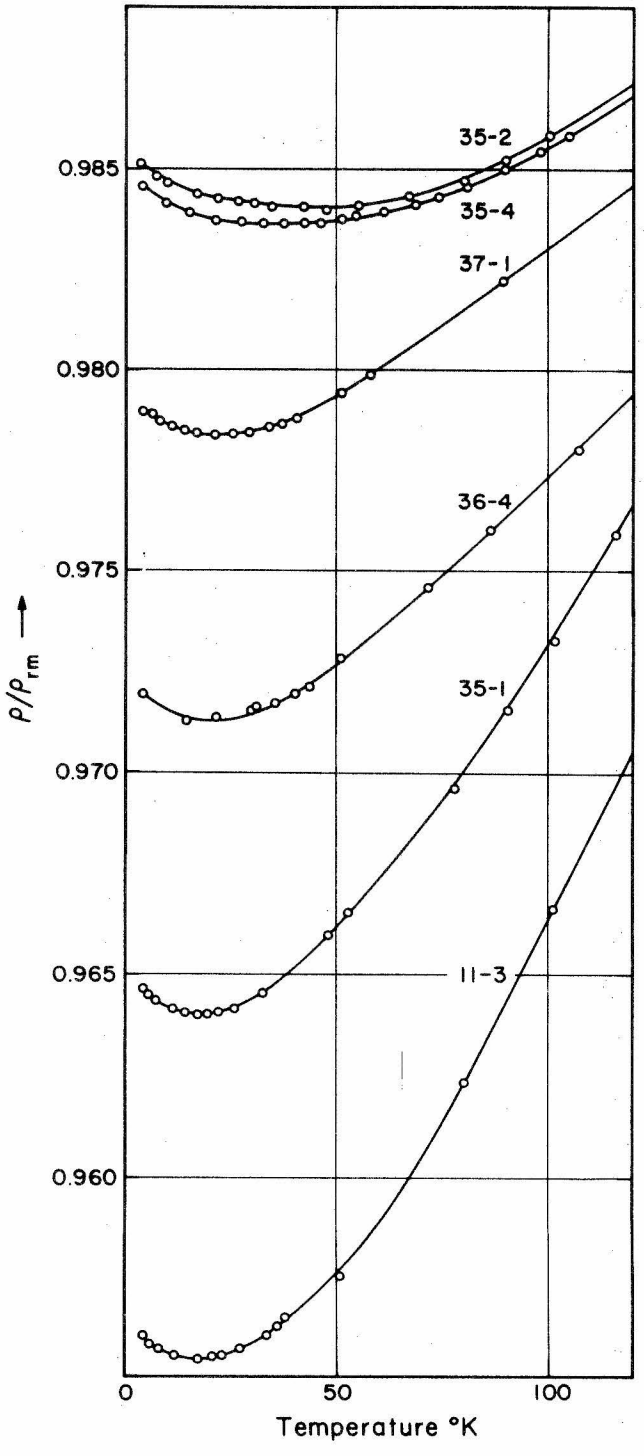

Fig. 8. The low temperature part of the relative electrical resistance versus temperature for six amorphous FePC foils.

specimen, and so does the temperature at which the minimum occurs. In addition, the residual resistance ratio also varies from specimen to specimen. It is believed that a small slope and a high residual resistance ratio are characteristic of the absence of microcrystals. It can also be seen from Fig. 8 that the minimum in the resistance curves decreases with an increase in the resistance temperature curve slope at $100^{\circ}K$, and thus, the effect of a small amount of a crystalline phase apparently decreases the temperature at which the minimum occurs. In an effort to find a correlation between these variables, the results obtained on 14 different specimens, containing various amounts of a microcrystalline phase have been plotted in Fig. 9, 10 and 11. Figure 9 shows the ratios of the resistance at the minimum to that at room temperature vs. the minimum temperature. In Fig. 10, ratio of resistance at liquid helium temperature to that at the room temperature is plotted against the minimum temperature. In Fig. 11, the temperature coefficient of resistance at room temperature is shown vs. the temperature at the minimum. All these curves seem to converge to either a maximum or a minimum value which is believed to correspond to those specimens which are approaching the ideal amorphous structure. The minimum value for the slope of the resistance-temperature curve at room temperature would be about $0.7 \times 10^{-4}/^{\circ}C$. The maximum value for the ratio of resistance at liquid helium temperature to that at room temperature would be about 0.984. These values would be characteristic of the ideal amorphous FePC.

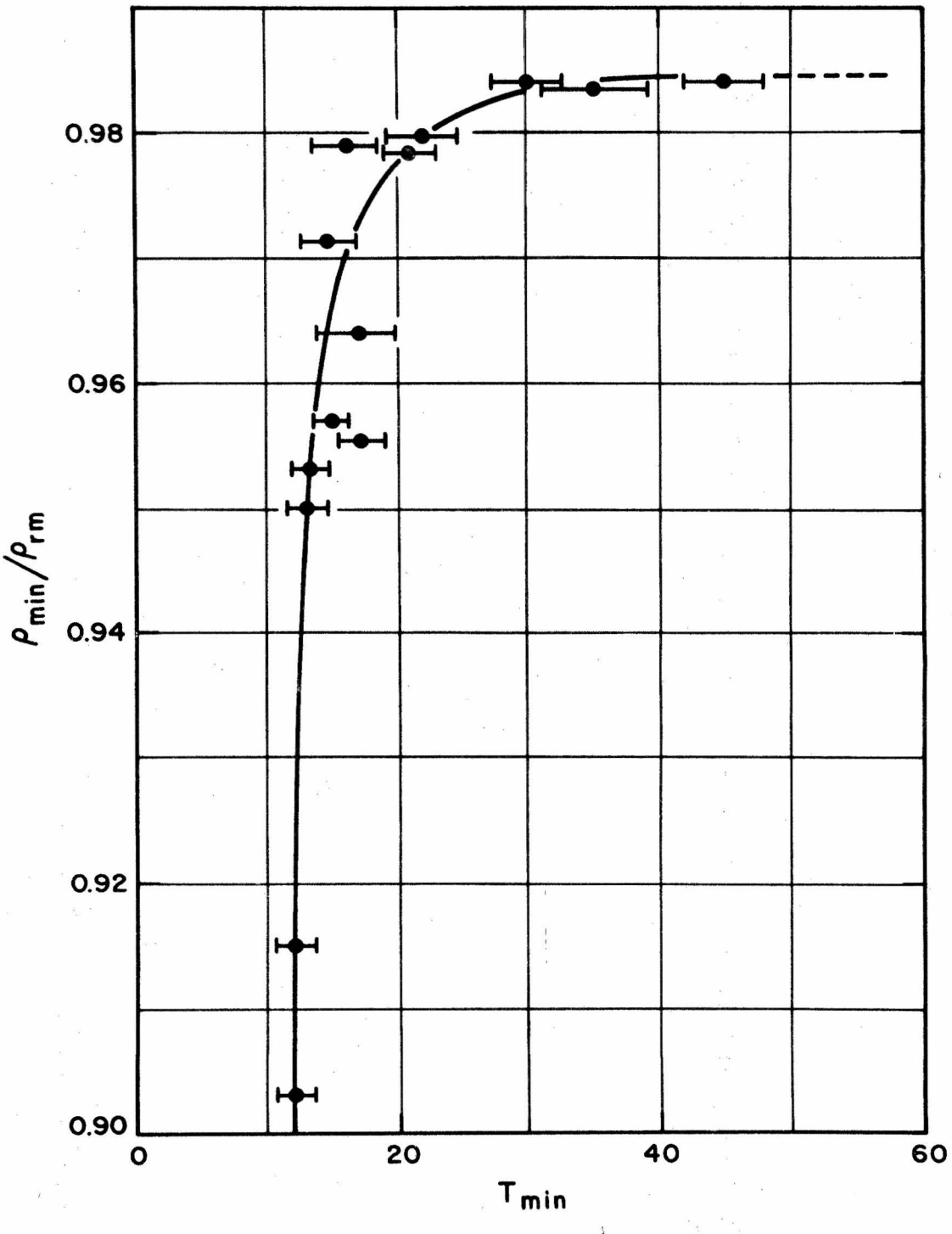

Fig. 9. Relative resistance at the resistance minimum (ρ_{min}/ρ_{rm}) versus the temperature at which the minimum occurs (T_{min}) for amorphous FePC foils.

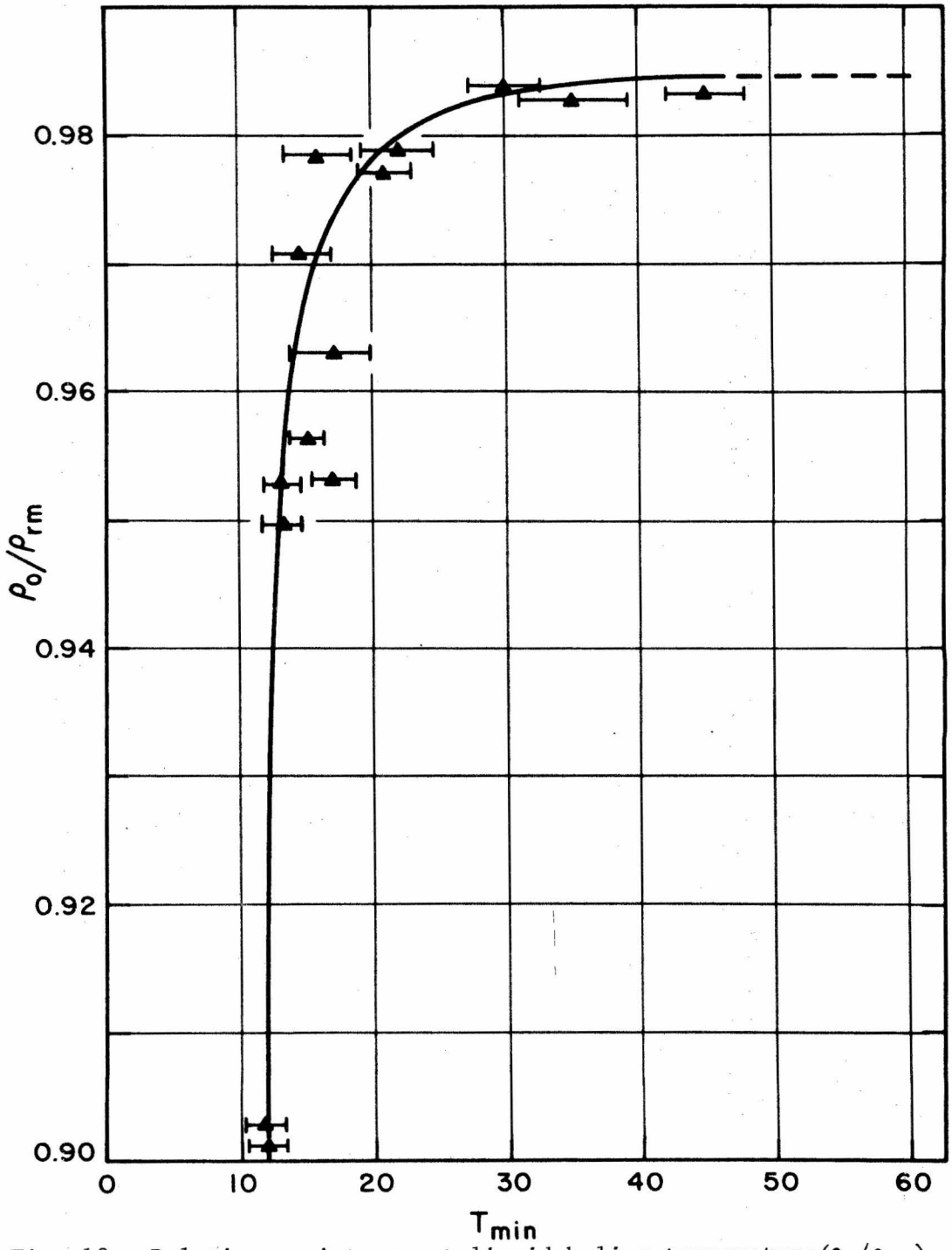

Fig. 10. Relative resistance at liquid helium temperature (ρ_o/ρ_{rm}) versus the temperature at which the minimum occurs (T_{min}) for amorphous FePC foils.

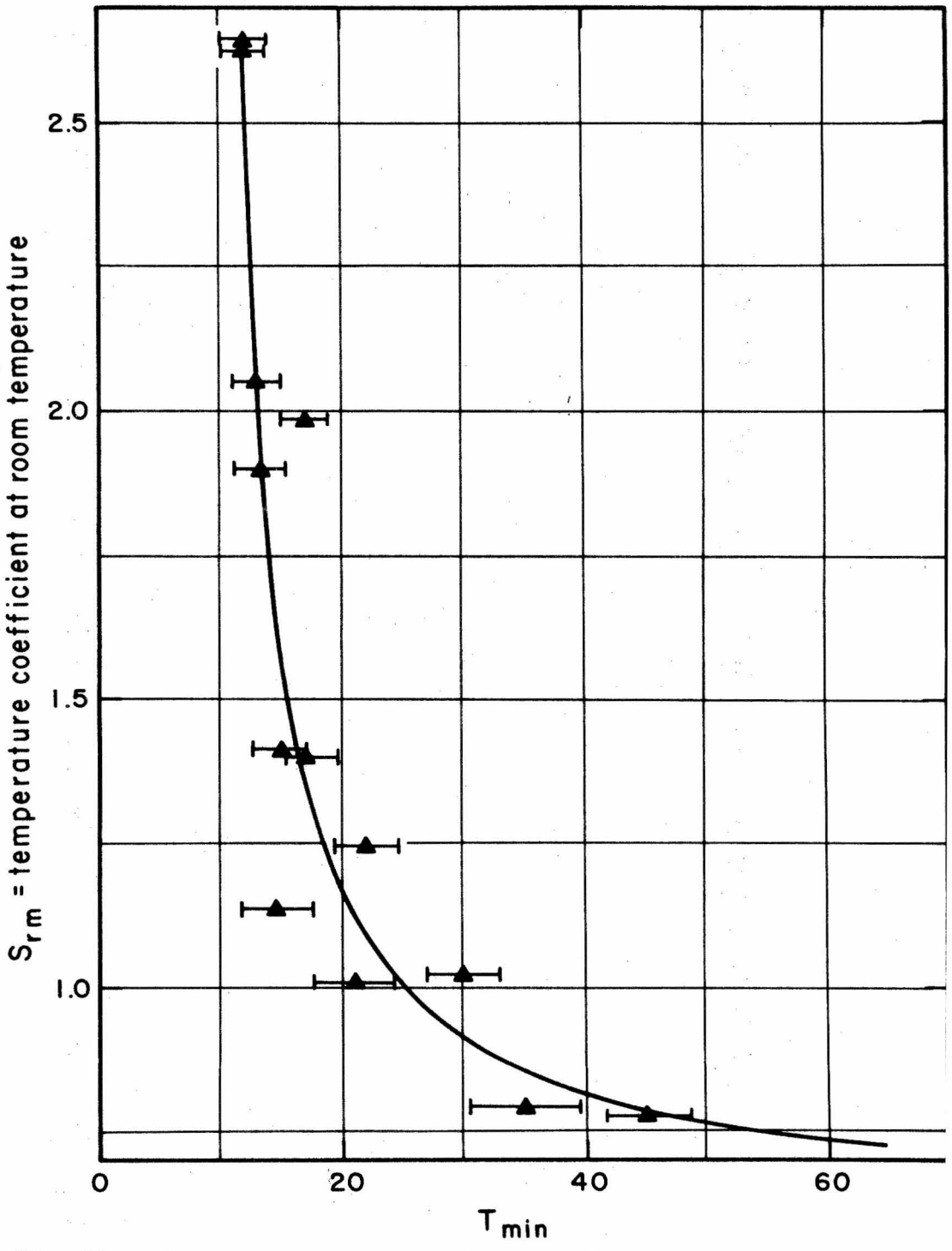

Fig. 11. The temperature coefficient of electrical resistance at room temperature versus the temperature at which the minimum occurs (T_{min}) for amorphous FePC foils.

C. Hall Effect and Magnetic Measurements

The results of the measurements of the Hall electric field per unit current density are shown in Figs. 12 and 13 for various temperatures ranging from 4.2°K to 350°C. From these plots, the Hall constant was determined from the slopes of the initial portions of the curves and are shown up to 300°K for two specimens in Fig. 14 and also in Table II. The results obtained for a specimen taken to higher temperatures are shown in Fig. 15. The drop in the Hall constant above 550°K is related to the Curie temperature and will be discussed in section IV. Transverse magneto-resistance was measured at three temperatures on one of the Hall effect specimens and its variation with magnetic field is shown in Fig. 16. At 4.2 and 233°K, the magneto-resistance is negative up to the maximum field used, namely 9.5 kG. At room temperature the magneto-resistance is positive up to 3.5 kG and becomes negative at higher fields.

Although the amorphous FePC alloys rapidly transformed around 420°C, the crystallization rate is small below 350°C, and a Curie transition could be observed around 315°C. This transition was measured by the induction method and a typical curve is shown in Fig. 17. A curve recorded for pure nickel is shown in the same figure for the purpose of comparison. The temperature dependence of the bulk magnetization of the amorphous alloy measured with a null pendulum magnetometer and also by Mössbauer spectroscopy is shown in Fig. 18. From the bulk

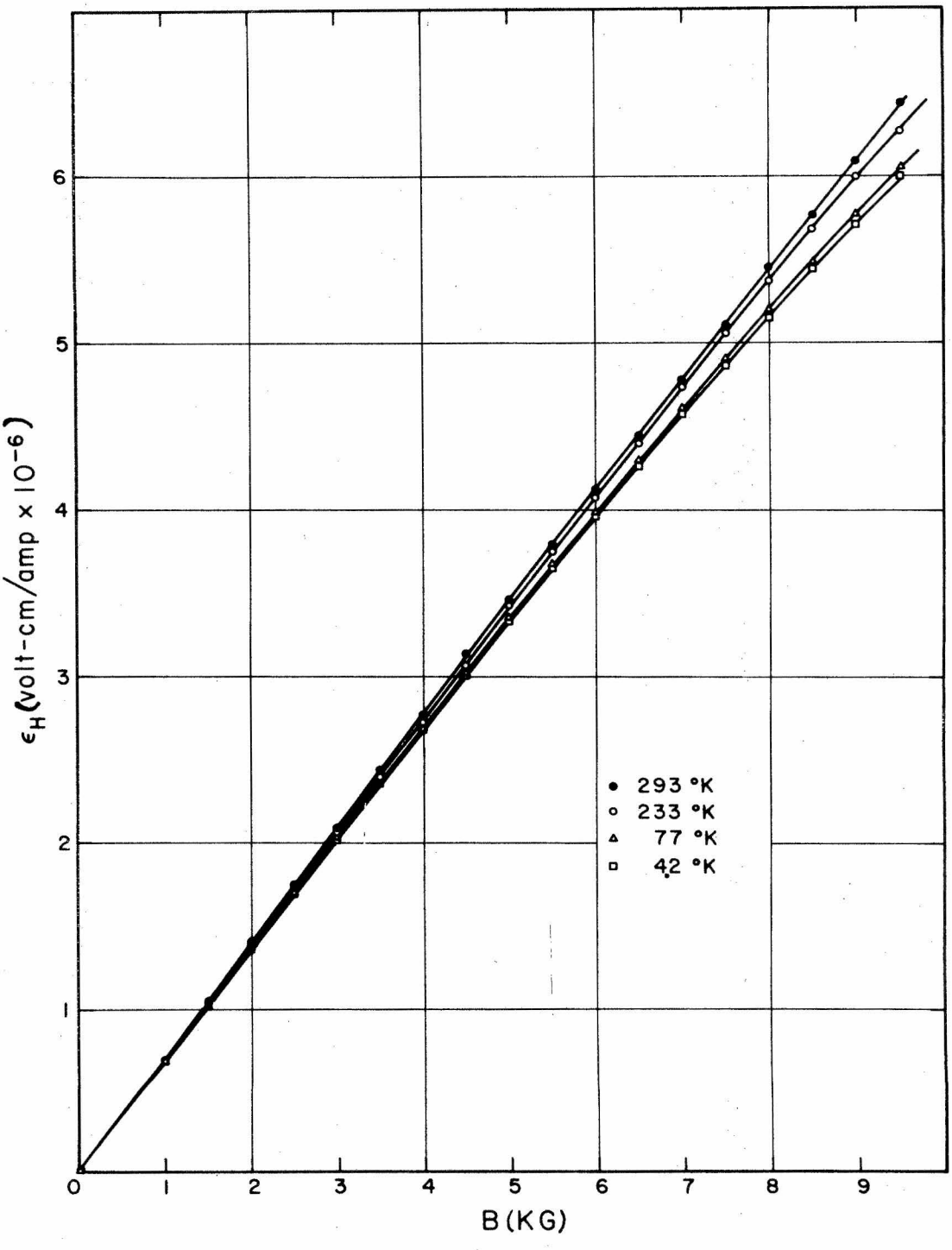

Fig. 12. Hall electric field per unit current density versus magnetic induction for low temperatures with maximum magnetic field of 10 kOe.

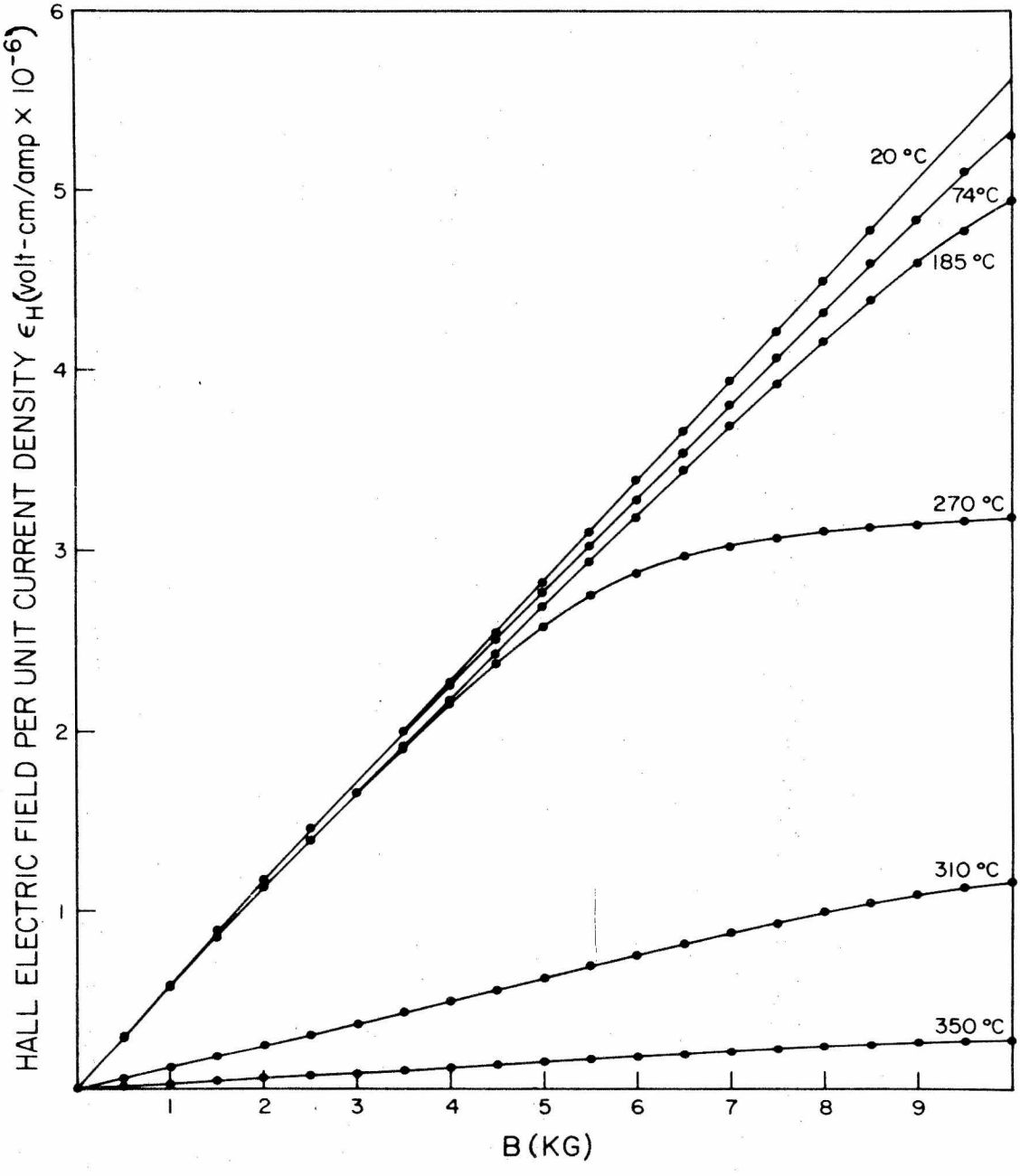

Fig. 13. Hall electric field per unit current density versus magnetic induction at high temperatures.

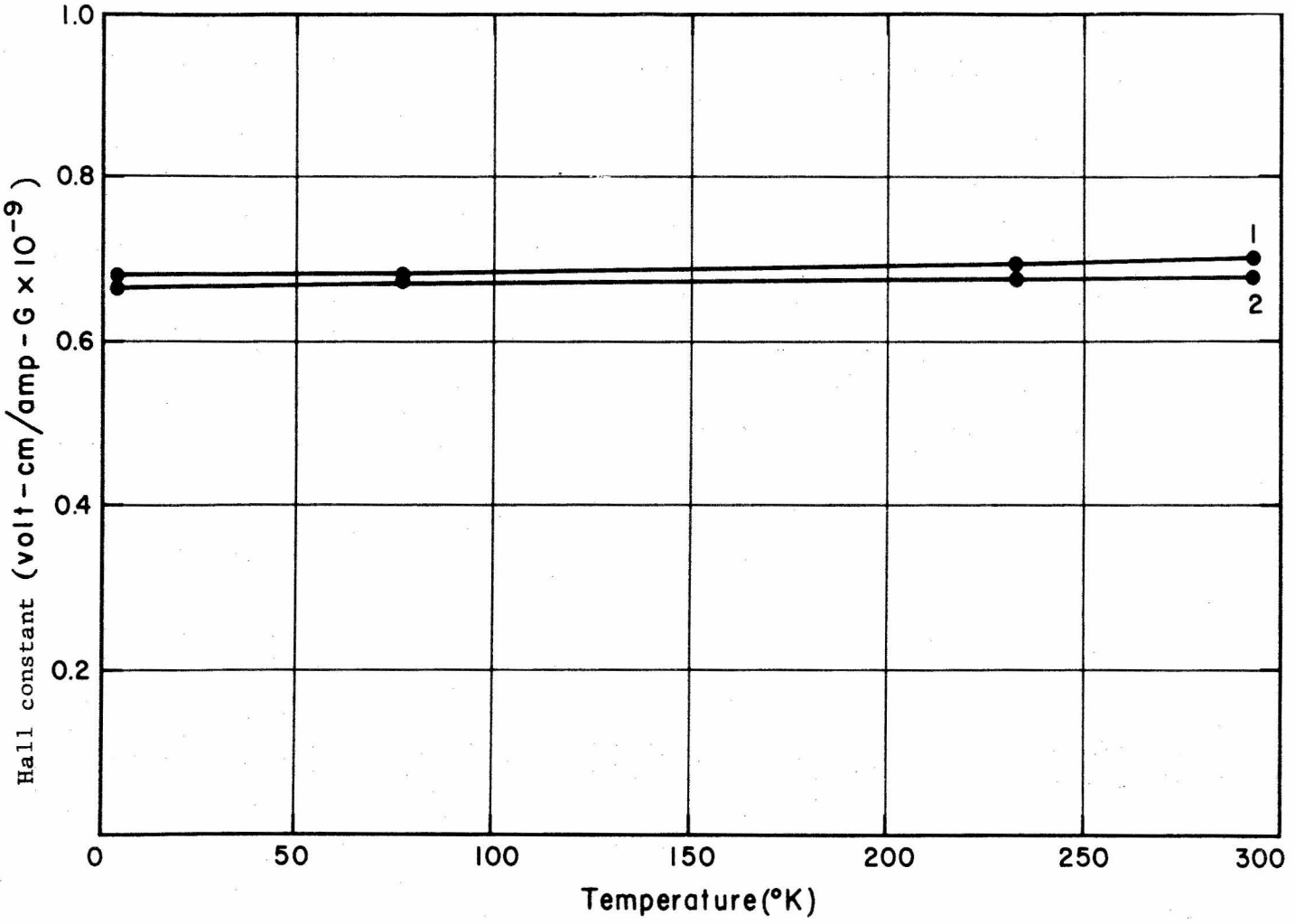

Fig. 14. Hall constant for amorphous FePC alloy determined from the slopes of the initial steep portions of the plots of Hall electric field per unit current density versus magnetic induction at low temperatures.

TABLE II

HALL CONSTANT OF TWO SAMPLES MEASURED AT LOW TEMPERATURES

Temperature	Hall Constant $R = \left(\frac{\partial \epsilon_H}{\partial B}\right)_{B=0} \times 10^{-9}$ volt-cm/amp-G	
	Sample 1	Sample 2
293°K	0.700	0.677
233°K	0.695	0.676
77°K	0.684	0.672
4.2°K	0.680	0.664
Temperature Coefficient of Hall Constant	$33 \times 10^{-6}/^{o}C$	$20 \times 10^{-6}/^{o}C$
Temperature Coefficient of Electrical Resistance	2.64×10^{-4}	2.0×10^{-4}

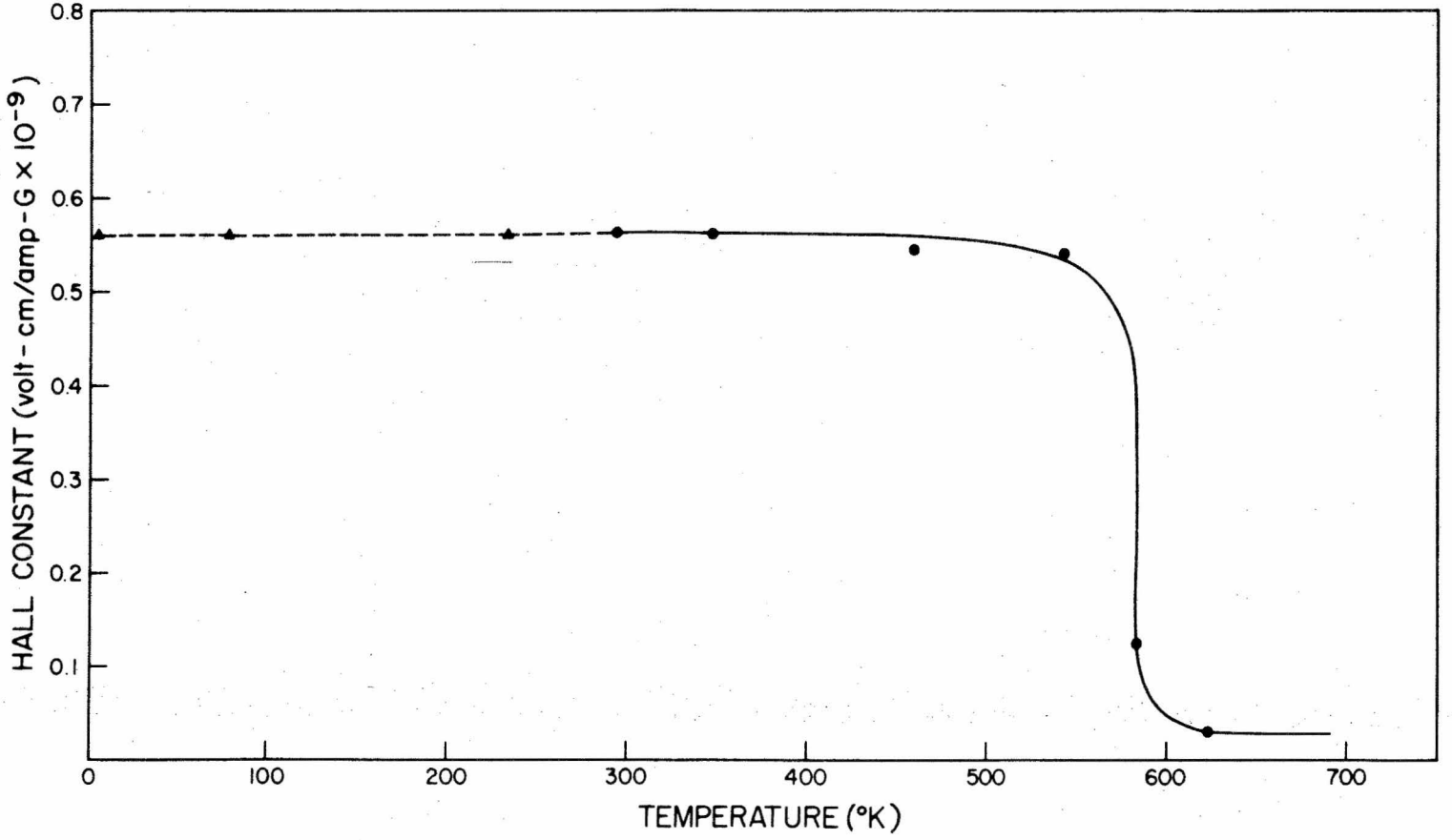

Fig. 15. Hall constant for amorphous FePC alloy determined from the slopes of the initial steep portions of the plots of Hall electric field per unit current density versus magnetic induction at high temperatures. Dotted line is extrapolated from Fig. 14.

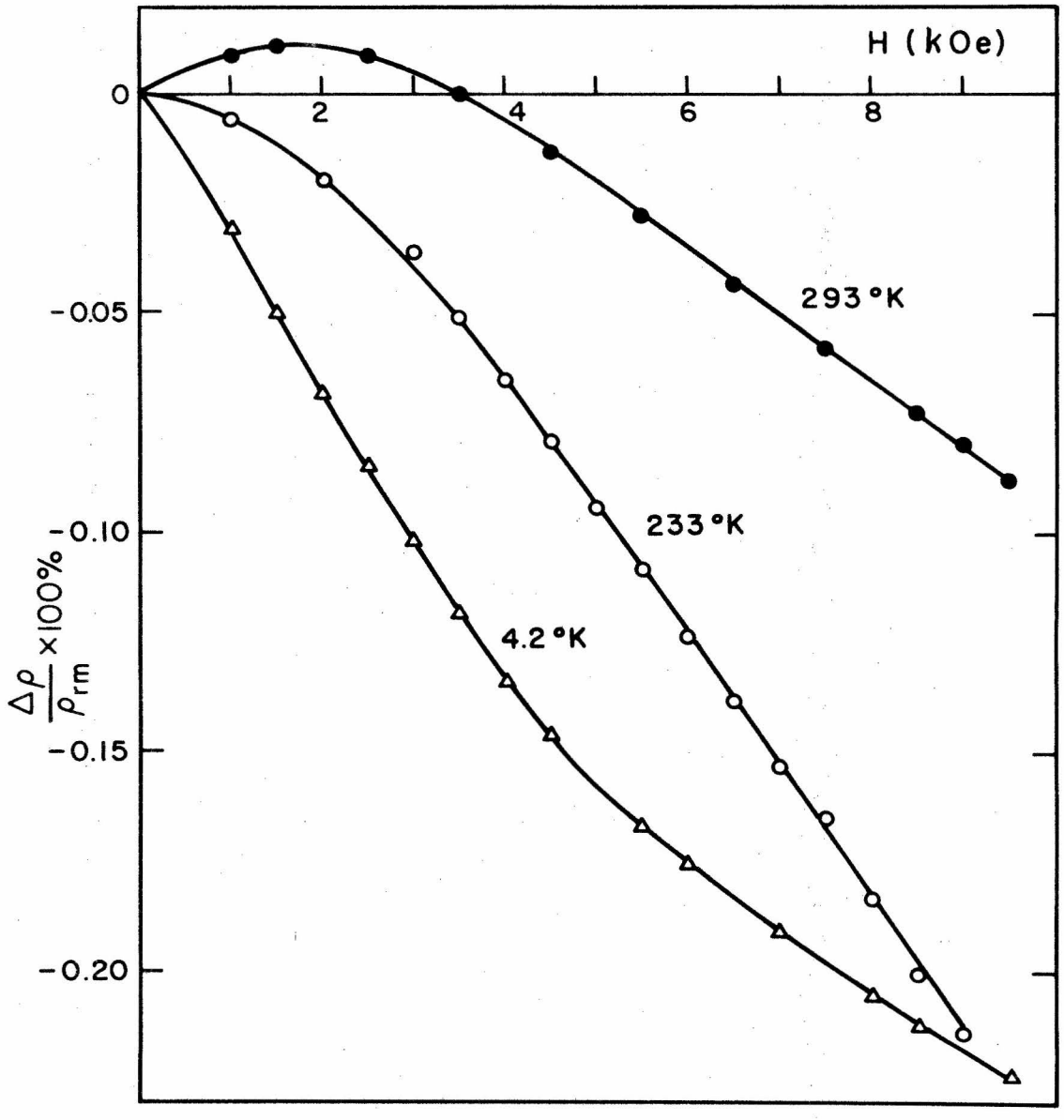

Fig. 16. Transverse magneto-resistance $\Delta\rho/\rho_{rm}$ versus magnetic field.

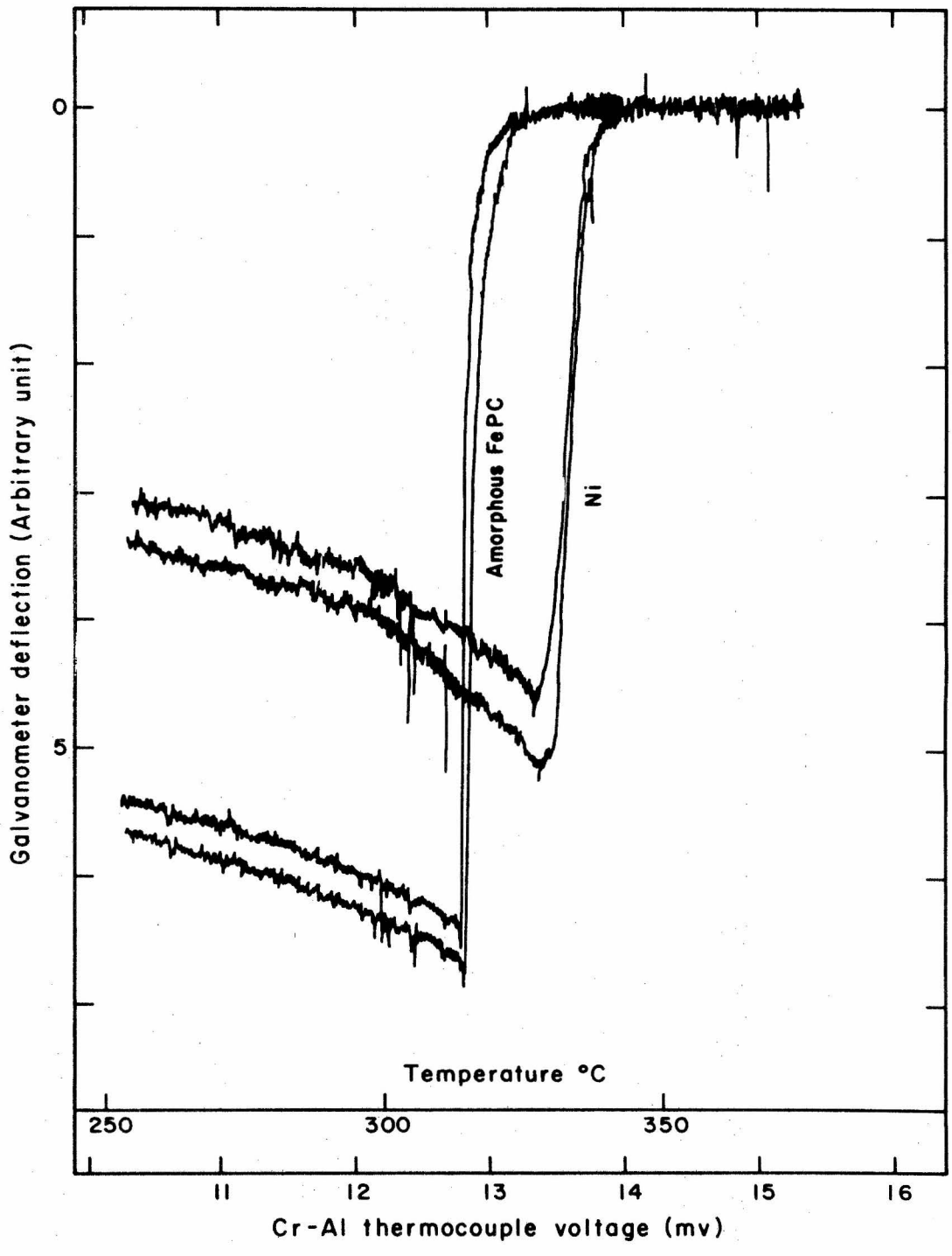

Fig. 17. Curie Temperature Records of Amorphous FePC Foil and of a N_i foil.

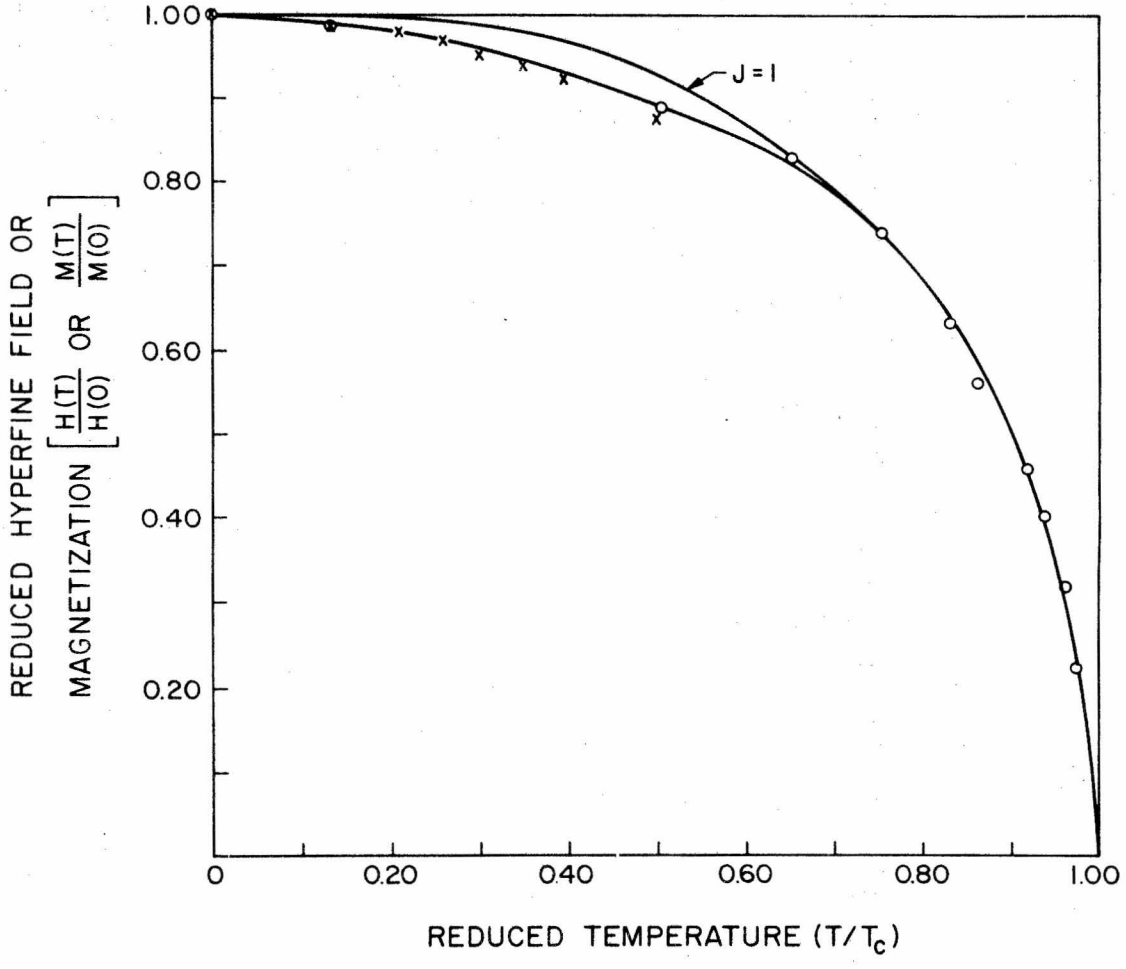

Fig. 18. Spontaneous magnetization (x) and average hyperfine field (o) of amorphous FePC alloy versus temperature (Ref.71).

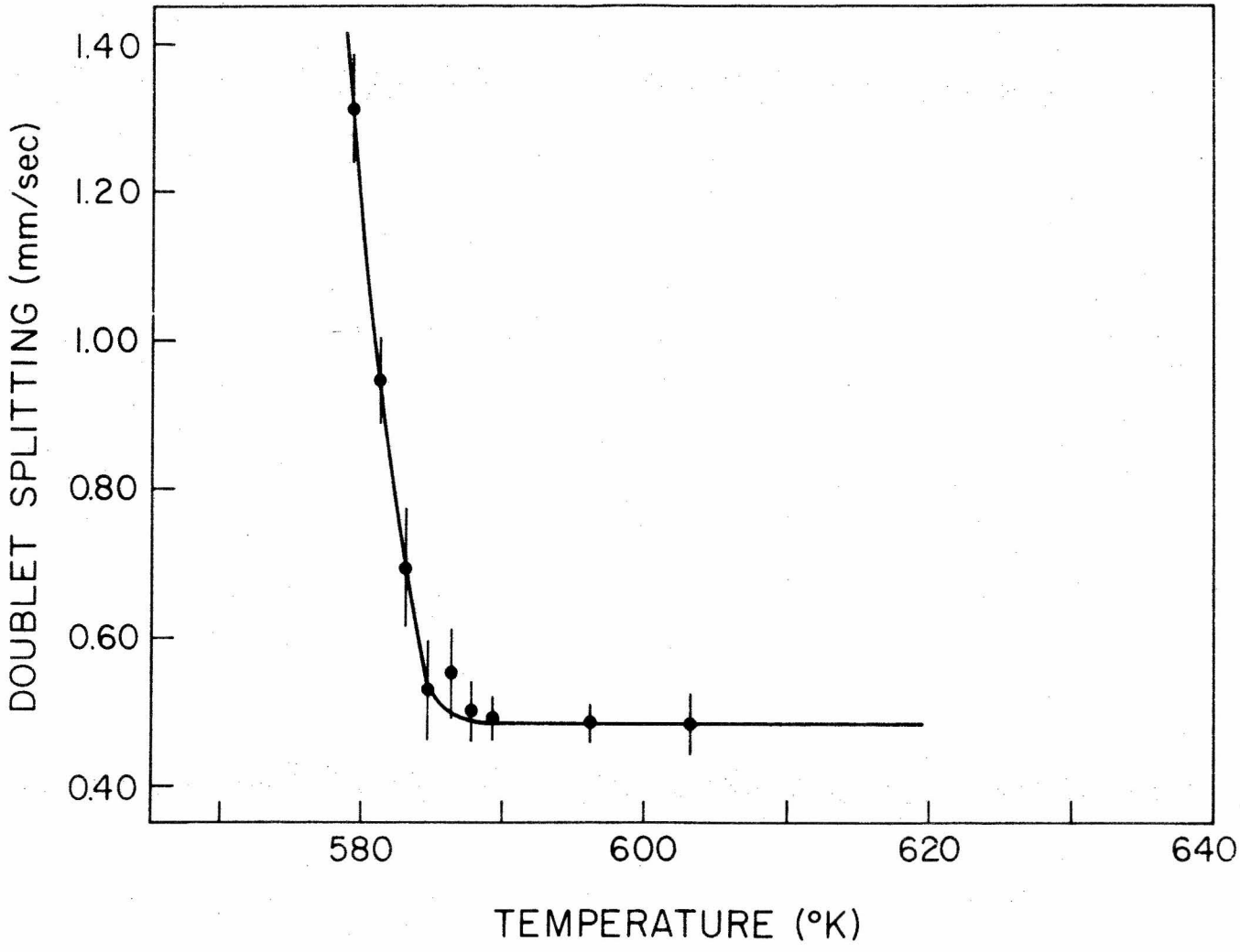

Fig. 19. The doublet splitting of Mossbauer spectra as a function of temperature during the Curie magnetic transition (Ref.71).

magnetization measurements made between 1.8 and 300°K and their extrapolation to 0°K, the magnetic moment per iron atom was found to be $2.10 \pm 0.01\mu_\beta$. The Mössbauer spectra obtained at temperatures between 570 and 590°K were fitted with a two peaks pattern and the splitting of the components assumed to be proportional to the hyperfine field was plotted as a function of temperature (Fig. 19). The Curie temperature deduced from this plot is 586 ± 2°K, in good agreement with that measured by the induction method (588 ± 1°K).

IV. DISCUSSION

A. The Structure of Amorphous Solids

Many experimental and theoretical studies have been published on the structure of silicate glasses. These studies have a bearing on the present subject because it is believed that the structure of amorphous alloys obtained by rapid quenching from the liquid state is indeed very closely related to that of glass. Besides, the analogy between the X-ray and electron diffraction patterns of the two classes of solids,[9,10] recent studies have shown that amorphous alloys do possess a "glass transition" and also behave like glass from the rheological point of view. By measuring the specific heat of an amorphous AuSiGe alloy, Chen and Turnbull[23] have established the existence of a glass transition in this alloy at about 290°K. The mechanical properties of the same alloy was studied under constant stress and in a temperature range from 285°K to 305°K, viscous flow was observed. Therefore, it seems logical to assume that the criteria which have been developed for glass formation in silicate systems should be applicable to metallic alloys.

About thirty years ago G. Hagg[24] suggested that the glassy state could be explained primarily on the basis of the structure of the liquid from which glass is formed rather than on the basis of the structure of the crystallized solid. The major difficulty in developing Hagg's ideas was the lack of knowledge concerning the liquid structure. Since then strong similarities have been found between the structure of the liquid

and that of the corresponding crystalline solid, especially from the point of view of short range order.[25,26]

The small differences between the structure of a glass and that of a liquid are difficult to study. The radial distribution function deduced from X-ray diffraction data is not accurate enough to give reliable and very detailed information beyond the first and second shells of neighboring atoms. The three numbers available with some reliability are the average distances of the first and second nearest neighbors, and the number of atoms in the first nearest neighbor shell. These numbers are quite reliable for liquids and amorphous solids consisting of one kind of atoms. An interesting correlation has been obtained between the ratio of second nearest neighbors (r_2) to that of first nearest neighbors (r_1) and the state of the element, namely crystalline, amorphous or liquid. The available data found in the literature have been compiled and are presented graphically in Fig. 20 and data for amorphous solids are also given in Table III with appropriate references. The number of amorphous elements shown in Fig. 20 is obviously limited and some comments are in order on how the r_2/r_1 ratios assigned to them were obtained. For amorphous Te, the ratio was obtained by extrapolating the results found for quenched Te-In alloys.[10] For Pd, it was obtained from the results reported on amorphous $Pd_{80}Si_{20}$ alloys.[9] For Fe, the value deduced from the FePC alloys described in the present study was not far from that deduced from vapor deposited amorphous films.[20] The data for Pb were taken from a study

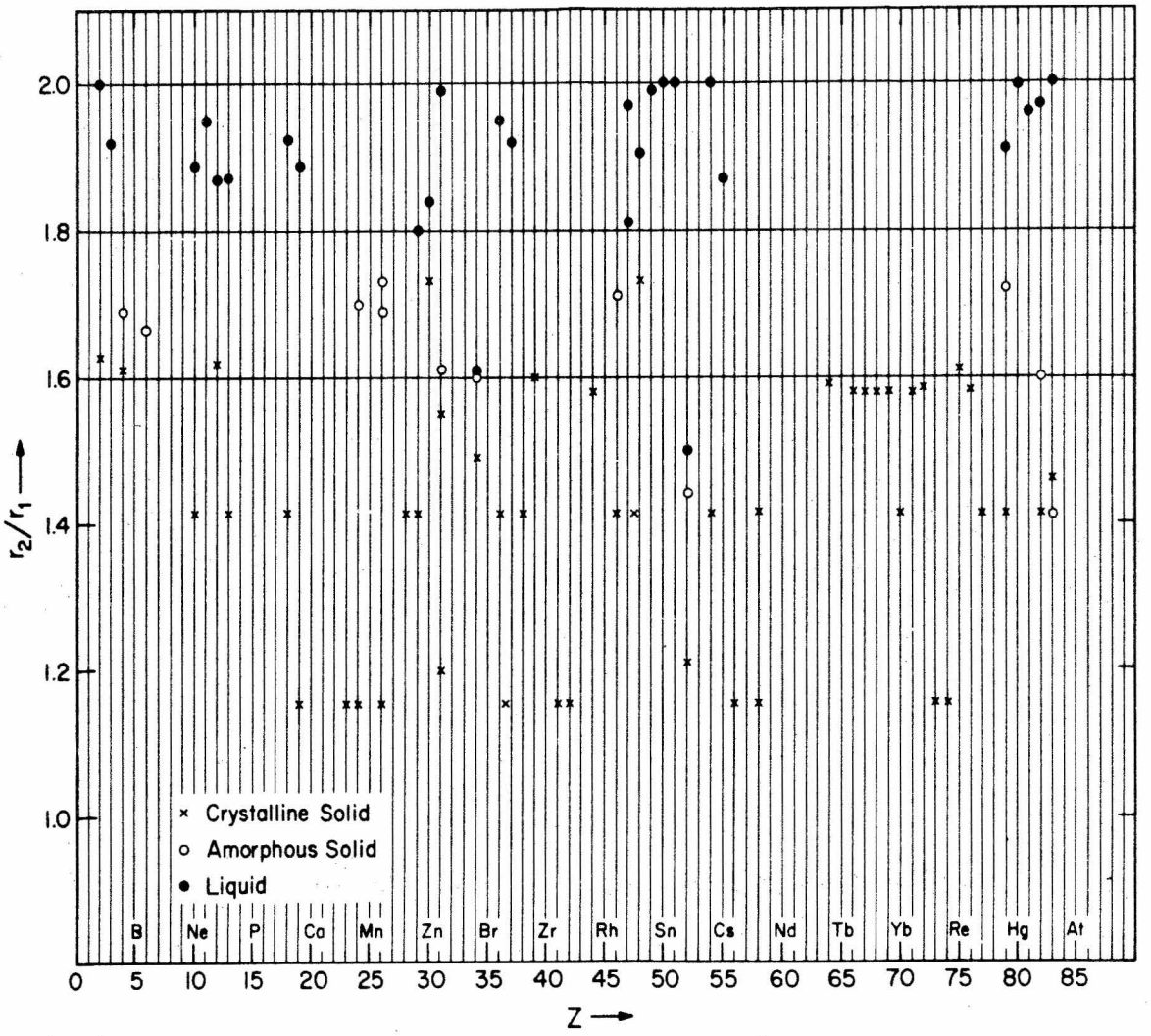

Fig. 20. Summary of ratios of second to first nearest neighbors distances (r_2/r_1) for liquid amorphous and crystalline elements.

TABLE III

SUMMARY OF RATIOS (r_2/r_1) OF THE SECOND TO FIRST NEAREST NEIGHBOR DISTANCES FOR AMORPHOUS ELEMENTS

Atomic No.	Sub-stance	Prep. Math.	Anal. by	Stable below °K	Anal. at °K	r_1 Å	r_2 Å	r_2/r_1	Ref.
83	B_i	v	e	20	4.2	3.28	4.5	1.37	33
83	B_i	v	e	--	4.2	3.32	4.7	1.41	34
31	G_a	v	e	90	4.2	2.86	4.6	1.61	33
31	G_a	v	e	90	77	2.84	4.4	1.55	33
4	B_e	v	e	130	4.2	2.25	3.7	1.64	27
4	B_e	v	e	130	77	2.25	3.8	1.69	27
6	C	v	e	--	293	1.5	2.5	1.67	35
24	Cr	v	e	220	4.2	2.64	4.5	1.70	20
34	Se	ℓ	x	--	298	2.34	3.75	1.60	36
26	Fe	v	e	180	4.2	2.60	4.50	1.73	20
26*	$Fe_{80}P_{13}C_7$	ℓ	x	690	293	2.60	4.40	1.69	--
82*	$PbBi_{12}$	v	e	--	4.2	3.25	5.2	1.60	27
46*	$PdSi_{20}$	ℓ	x	$\sim$ 600	293	2.79	4.78	1.71	9
79*	Au-Co	v	e	273	77	2.85	4.90	1.72	29
47*	Ag-Cu	v	e	273	77	2.9	$\sim$ 5.0	$\sim$1.7	28
52†	Te	ℓ	x	$\sim$ 500	293			$\sim$1.44	10

v = vapor-deposited, ℓ = quenched from the liquid state
e = analyzed by electron diffraction, x = analyzed by X-ray diffraction
*Assuming that the first two peaks in the radial distribution function are mostly influenced by the major heavy element, i.e. Fe in $Fe_{80}P_{13}C_7$, Pb in $PbBi_{12}$, Pd in $PdSi_{20}$, Au in Au-Co, Ag in Ag-Cu.
†This is obtained by extrapolating the data from series of TeIn alloys in the indicated reference.

of vapor deposited films of a PbBi alloy[27] containing 12% Bi, and here again the ratio may be in error because of the presence of Bi in the alloy.

For Ag and Au, the location of the Ag-Ag and Au-Au peaks in amorphous vapor deposited alloys Ag-Cu[28] and Au-Co[29] were taken for the calculation. As shown in Fig. 20, there seems to be a correlation between the ratio r_2/r_1 and the state of the element. In the crystalline state the ratio is below 1.6, and is between 1.8 and 2.0 for the liquid state,[30] while the amorphous solids seem to occupy the range between 1.6 and 1.8. The r_2/r_1 data from various experimental and theoretical liquid models are shown in Table 4. As expected, such a correlation is not perfect. Two crystalline elements are definitely out of line, namely, Zn and Cd. This may be due to the abnormal axial ratio (1.85 and 1.89) for these two hexagonal closed-packed solids. Two liquids, namely, Se and Te are also outside of the normal range, and this may be the reason why these liquids have been called "crystal like" by some investigators.[31,32]

Various studies have shown that the positions of the peaks in the radial distribution functions for liquid metals and alloys do not vary with temperature. For instance, radial distribution functions of liquid Ga have been studied over 50° range of centigrade temperature including 30° undercooling.[45] The r_2/r_1 ratio stays practically the same at 1.99. The r_2/r_1 ratios measured for amorphous Ga solid (vapor quenched) by Fujime[33] at helium and nitrogen temperatures are the same

TABLE IV

RECENT CALCULATIONS OF r_2/r_1 BASED ON VARIOUS LIQUID MODELS (Ref. 30)

Model	Methods	r_2/r_1	Ref.
Experimental Model	Two dimensional shaking experiment	1.9	38
	Three dimensional shaking experiment	1.9	39
Numerical Methods	Monte Carlo Methods	1.8	40
	Statistical Geometrical Model	1.9	41
Solution of Integral-equations	Collective Coordination techniques	1.89	42
	Chain equation	1.93	43
	Brown-Green-Yvon-equation	> 2.0	44

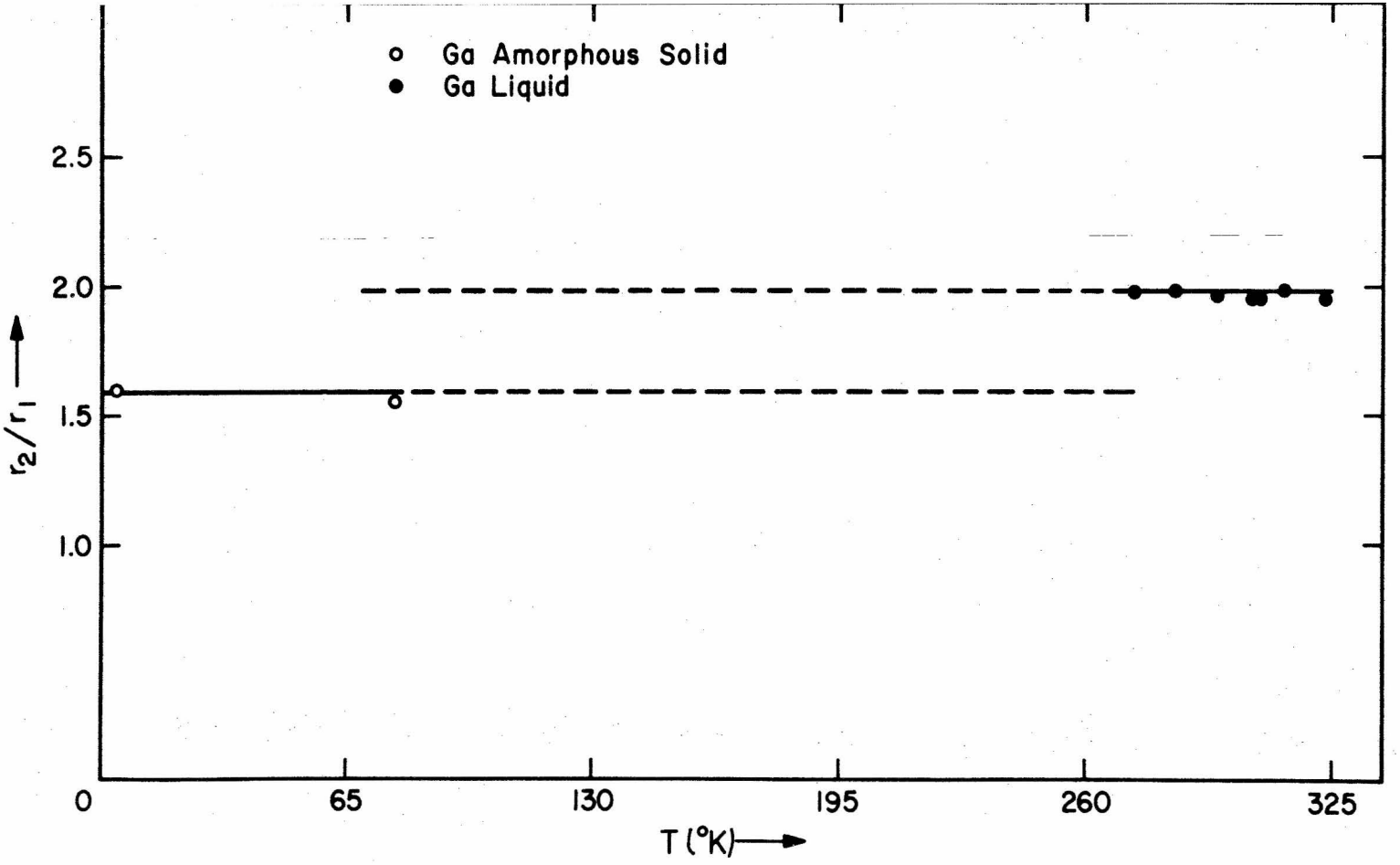

Fig. 21. Ratios of second to first nearest neighbors distances in function of temperature

at 1.58 ± 0.03. Fig. 21 shows the r_2/r_1 values more clearly in function of the temperature. From previous discussions liquids and glasses (or amorphous solids) are possibly characterized with their own fine structure which is pretty much independent of temperature. Thus a structure transition, at least of second order, must take place at some temperature, so that the fine structure will change from $r_2/r_1 = 1.9$ for liquids to $r_2/r_1 = 1.7 \pm 0.1$ for amorphous solids, i.e. gallium should have the glass-liquid transition temperature somewhere between 77°K and 273°K to accord with the prediction of Cohen and Turnbull[46] that glass transition will occur in all systems, including monatomic ones, if crystallization is bypassed. Recently Chen and Turnbull[23] found the evidence of glass-liquid transition in specific heat and viscosity measurements on ternary amorphous alloy Au-Si-Ge; the high viscosity close to the transition temperature was shown to depend primarily on the configuration rather than the temperature itself. The glass transition has not yet been studied in FePC amorphous alloys.

B. The Structure of Amorphous FePC Alloys

The model proposed by Bernal[41] to explain the structure of liquids is also applicable to amorphous solids. In his geometrical model, the atoms are located at the apices of a set of polyhedra whose center is not occupied by an atom (empty polyhedra). These polyhedra form a continuous but irregular network. A model for amorphous fused silica based on the same approach was developed by Zachariasen.[37] In this particular case, the polyhedra are tetrahedra. According to

Bernal, only five kinds of polyhedra would be possible to explain the liquid state. These are: tetrahedron, octahedron, trigonal prism, Archimedean antiprism and tetragonal dodecahedron. An attempt will now be made to show that in the case of amorphous FePC, the most probable structural polyhedron is the trigonal prism.

In the equilibrium condition, the FePC alloy contains three phases, namely Fe (with a small amount of carbon in interstitial solid solution), Fe_3P and Fe_3C. The compound Fe_3P, may not be the only one to consider, since in the Fe-P phase diagram (see Appendix I) the most stable compound at high temperature is Fe_2P, and Fe_3P which forms through a peritectic reaction can be very easily suppressed even by slow cooling from the melt. Therefore it can be assumed that if there is any local ordering present in the liquid state, such an ordering would either be the result of Fe-Fe bonds and Fe-P bonds similar to those existing in Fe_2P, or Fe-C bonds. The radial distribution functions for Fe-Fe correlation were calculated for Fe_2P, Fe_3P and for b.c.c. Fe (see Appendix III). In the latter case the crystalline structure was randomnized by displacing the atoms from their crystalline position at random as explained in Appendix III. The results of these computations are shown in Fig. 22. When these curves are compared with that obtained for amorphous FePC, it is apparent that the short range configuration obtained for Fe_2P is very close to that relative to the amorphous alloy. In view of these results, the atomic arrangement present in Fe_2P is very

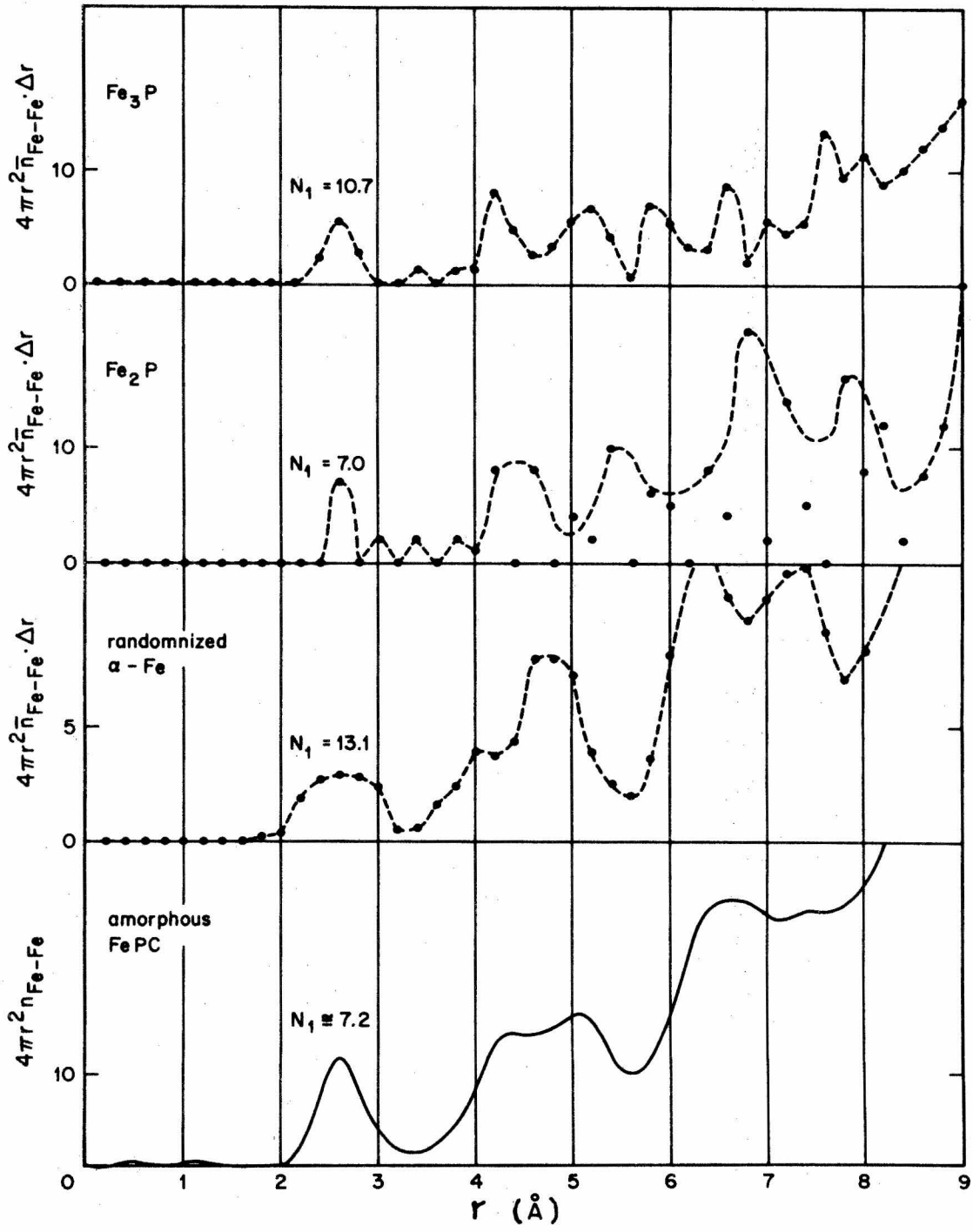

Fig. 22. Radial distribution functions for Fe-Fe correlation in Fe_3P, Fe_2P and randomnized α-Fe, Δr = 0.2Å.

close to that relative to the amorphous alloy. In view of these results, the atomic arrangement present in Fe_2P will be discussed.

The crystal structure of Fe_2P[47,48] (Type C_{22}) is haxagonal with a = 5.865 Å, c = 3.456 Å and is shown in Fig. 23. The iron atoms are arranged in trigonal prisms stacked on their triangular bases and aligned along the [110] direction. This is shown in Fig. 24. There are two kinds of prisms with triangular edges of lengths 2.60 and 3.08A, and every prism has one phosphorus atom in its center. The three rectangular faces of the larger prism are capped with half octahedra (edge length 2.63A) whose apex (iron atom) is one of the three points of the larger prisms. The larger prism's triangles contact each other and form a continuous network by sharing an iron atom between two triangles on two prisms. The interatomic distances in Fe_2P crystals are:

PI	3 Fe I	2.22	PII	6 Fe I	2.29
	6 Fe II	2.48		3 Fe II	2.38
FeI	2 P I	2.22	FeII	1 P II	2.38
	2 P II	2.29		4 P I	2.48
	2 Fe I	2.60		2 Fe I	2.63
	2 Fe II	2.63		4 Fe I	2.71
	4 Fe II	2.71		4 Fe II	3.08

The designations Fe I, Fe II, P I, P II are shown in Fig. 24.

Since the presence of carbon in the liquid alloy appears to be an important factor in obtaining an amorphous solid, its crystalline structure will also be discussed. The compound Fe_3C (cementite) is orthorhombic with a = 13.548Å, b = 15.231Å, c = 20.181Å. As shown in Fig. 25, the iron atoms are reasonably close packed, each having either

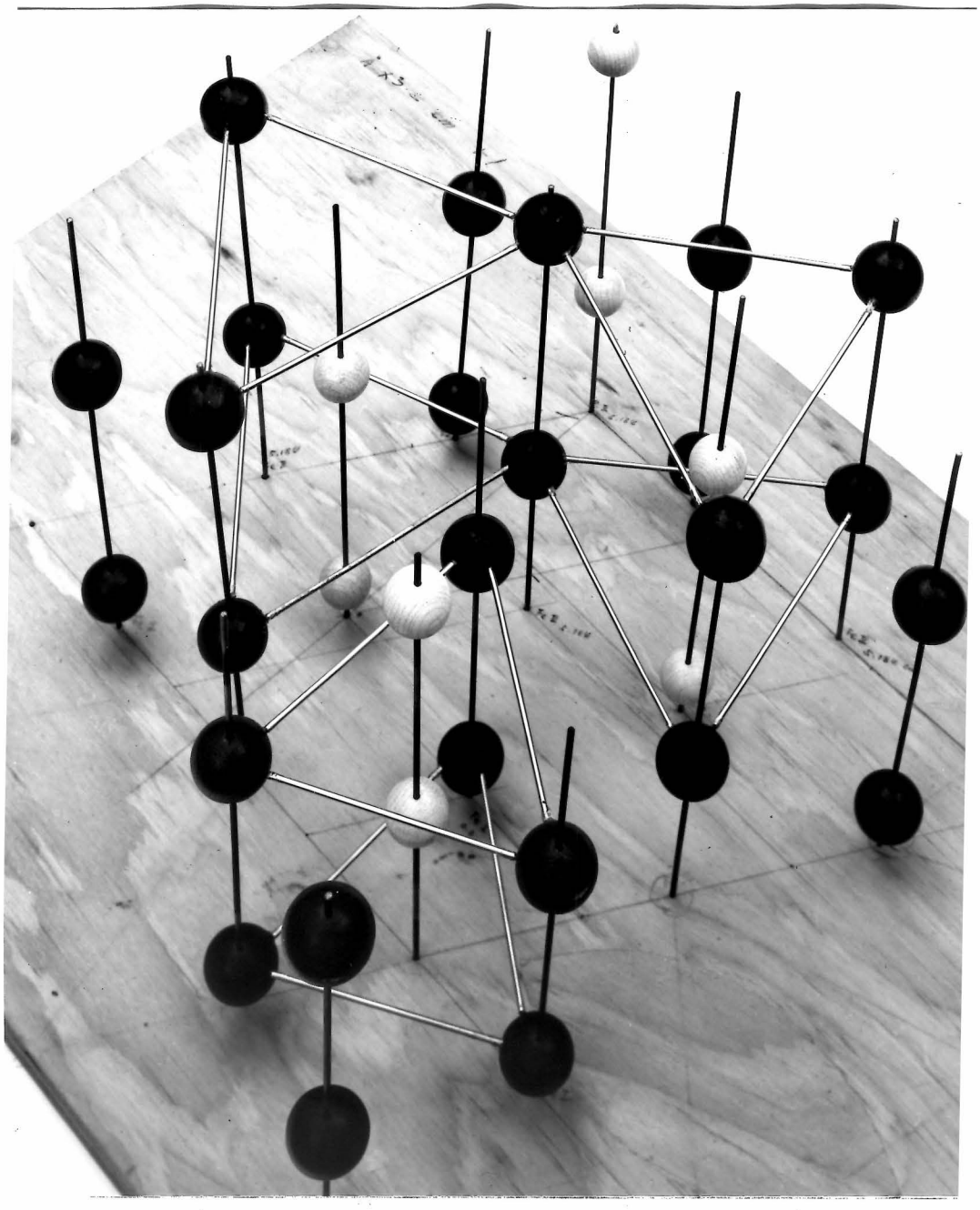

Fig. 23. Structure of Fe_2P compound.
Fe : larger black ball
P : smaller white ball

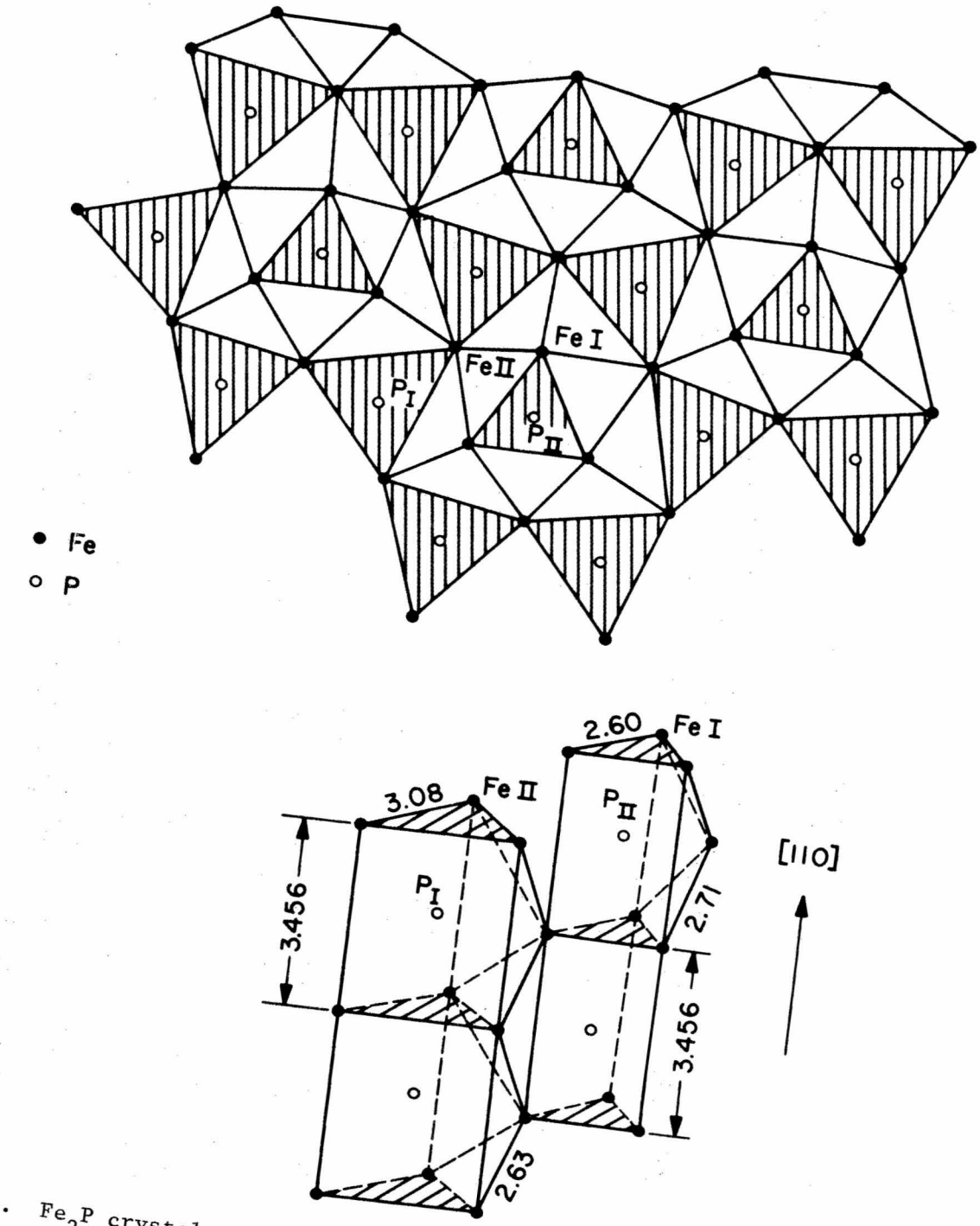

Fig. 24. Fe_2P crystal as viewed from [110] direction and relation of the two prisms of different size.

twelve iron neighbors at an average distance 2.62A or eleven at an average distance 2.58A. Each carbon is at the center of a trigonal prism of six iron atoms with the average Fe-C distance equal to 2.01A.[49,50] Series of trigonal prisms aligned along the [101] directions are in line contact, i.e. two prisms share two atoms on the edges of triangles as shown in Fig. 26 (A-A or A'A'). The angle between a prism and the next one on the same line is approximately 148° instead of 180°, so that the B atom of the prism on the neighboring line becomes the apex atom of an approximately half octahedron capping the prism's rectangular face A-A-A'-A'.

Based on Pauling's electronegativity values,[51] the bonds Fe-P and Fe-C should both be highly covalent, with only 5% ionic character in Fe-P and 12% in Fe-C. From Fig. 24, it can be seen that the P_I atoms are strongly bound with the three nearest Fe_I atoms, and only loosely bound to the six Fe_{II} atoms in the prism. By substituting carbon for phosphorus in this structure it might be expected that a carbon would draw the six rather loosely bonded Fe_{II} prism atoms by trying to form a deformed Fe_3C prism, faultly but covalently stacked up with the deformed Fe_2P prism (Fe_I-P_{II}) face to face or edge to edge. The edge of the triangle face of Fe_2P prism is 2.60A and that of Fe_3C prism is 2.62A (in average). Due to the approximately 148° angle in the Fe_3C crystals and their similarity in structures, Fe_2P type and Fe_3C type prisms with predominantly short-ranged, localized[52] rigid covalent bonds between them will give rise to a highly distorted

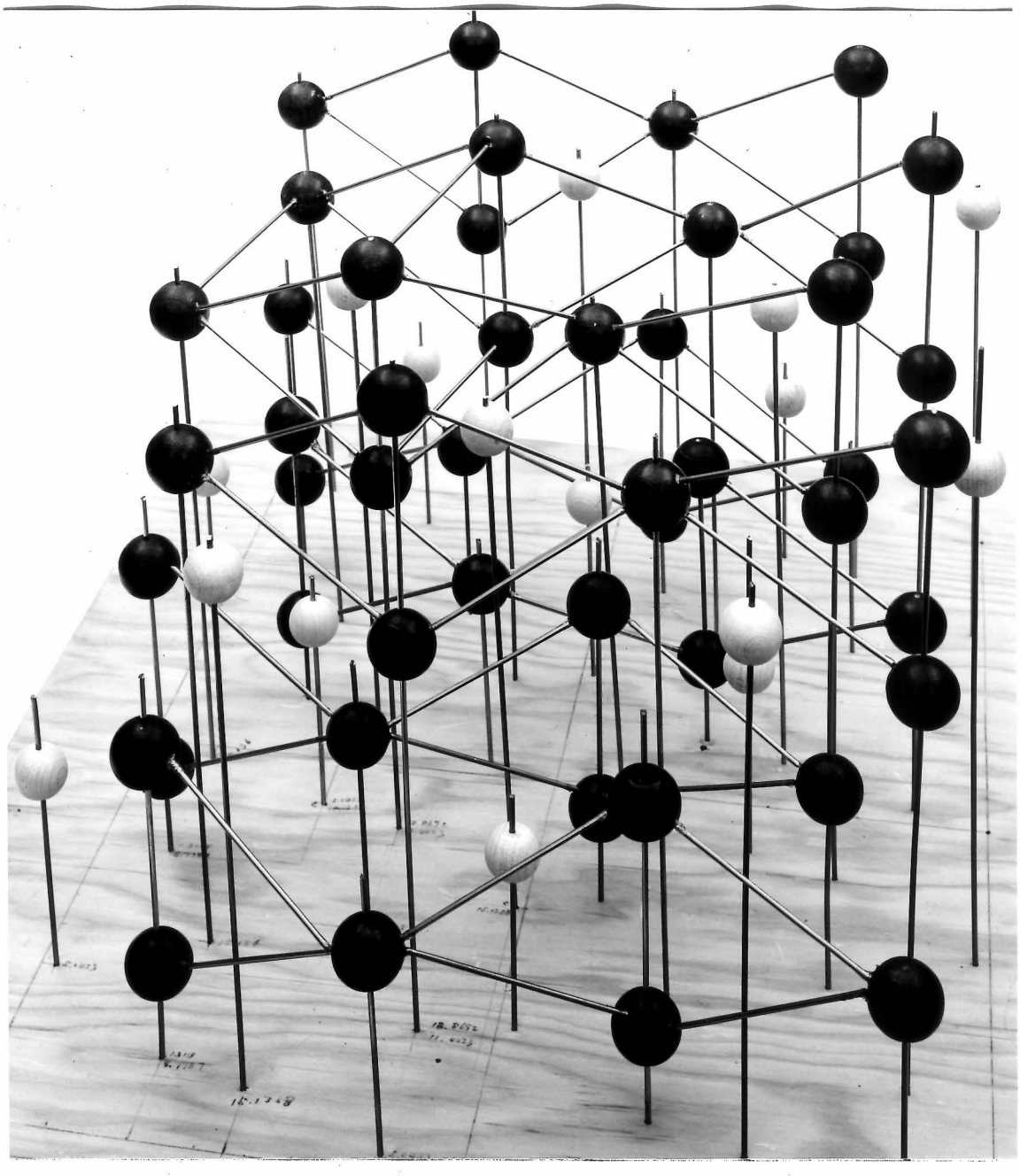

Fig. 25. Structure of Fe_3C compound.
Fe : larger black ball
P : smaller white ball

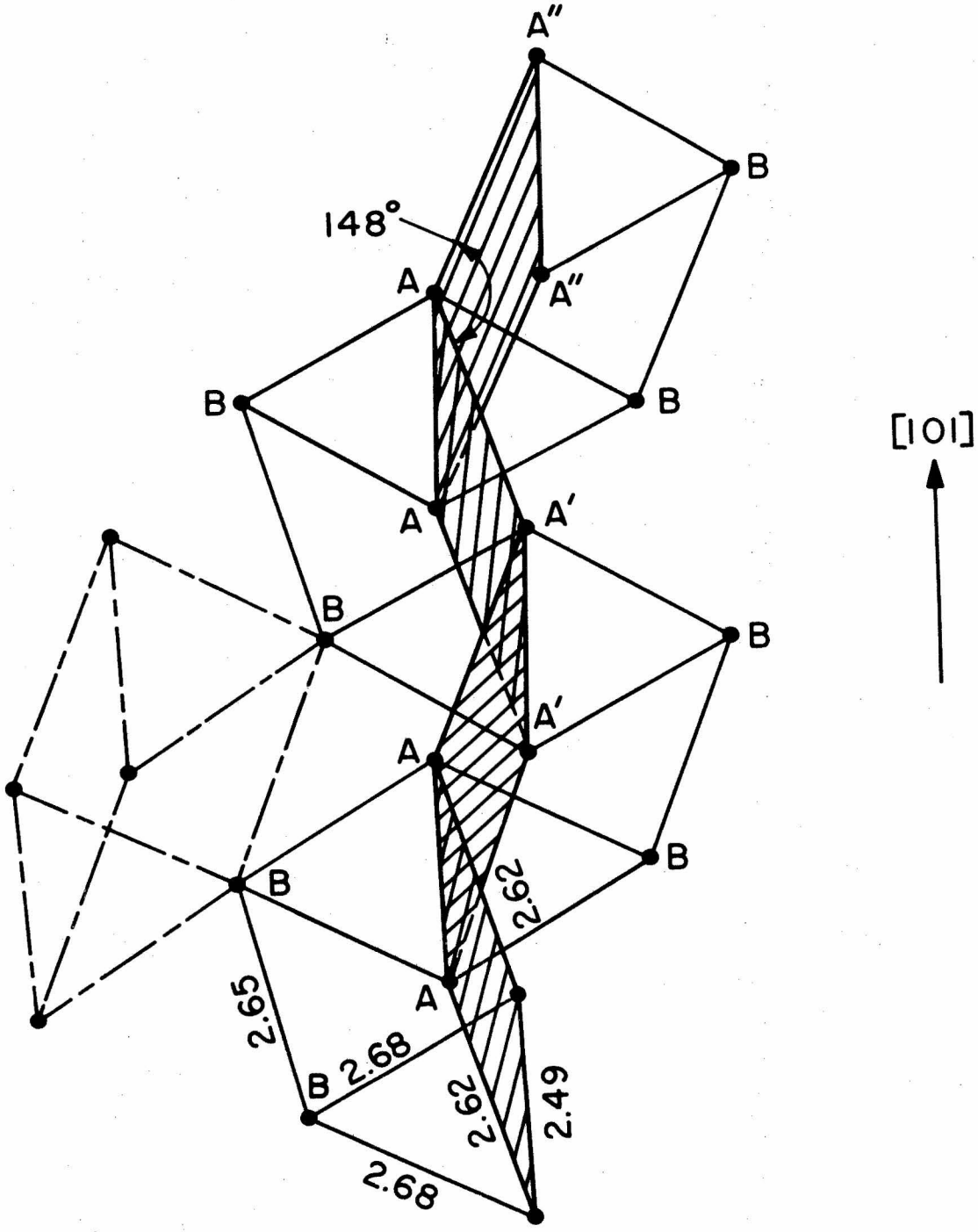

Fig. 26. Fe_3C structure in which iron atoms are located at corners of trigonal prisms. The prisms are lined up in zigzag along the [101] direction.

structure which makes long range periodicity impossible. Such a disordered array of trigonal prisms is a possible liquid state structure according to Bernal.[41]

The result of this analysis leads to the conclusion that the structure of amorphous FePC might be based on a combination of trigonal prisms similar to those existing in the crystal structures of Fe_2P and Fe_3C. The fact that in these crystalline structures the Fe atoms have an average ligancy of seven, is compatible with the results of the radial distribution function of amorphous FePC.

C. Electrical Properties

The electrical resistance of the amorphous alloy is characterized by a small temperature coefficient. Similar results have been previously reported in the case of amorphous Pd-Si alloys[9] and are explained by the fact that in such disordered structure most of the scattering is due to the random atomic arrangement and the contribution of thermal scattering to the resistivity is relatively small. The presence of a minimum in the resistance vs. temperature curve in the range of 10^{o} to 50^{o}K (Fig. 8) requires some comments. As explained in section IV.B. the temperature at which this minimum occurs is related to the slope of the resistance vs. temperature curve at 300^{o}K and also to the residual resistance, but these variations can be attributed to the presence of small crystals in the amorphous matrix. For specimens corresponding to an ideal amorphous structure this minimum would be very broad and located at much higher temperature. It is noted that the low resistance-ratio part of the curve in Fig. 9 or 10 and the high temperature coefficient part of the curve in Fig. 11 can be extrapolated to $\rho_o/\rho_{rm} = \rho_{min}/\rho_{rm} \approx 0.23$ at $T_{min} = 0$, and $S_{rm} \approx 8.0 \times 10^{-4}/^{o}C$ at $T_{min} = 0$, which is just how the crystallized FePC alloy behaves at low temperature. Minima in the resistivity of some dilute crystalline alloys containing a small amount of ferromagnetic atoms have been previously reported.[53] According to Kondo,[54] this minimum is a consequence of the interaction between spins of localized and conduction electrons. In Kondo's theory, the contribution of this interaction to the resistivity is proportional to $c(J/E_f) \log T$, in which c is the concentration

of the magnetic atom which is responsible for the local moment. Measurements on amorphous alloys containing dilute concentrations of iron, would be necessary to check this theory. However, the range of iron concentration within which an amorphous structure can be obtained by liquid quenching is very narrow, and there is little hope of checking the Kondo theory with this approach. In addition, it is very probably that the factor J, is greatly affected by the presence of microcrystals resulting of an imperfect quench.

The most important result obtained from the measurements of the ordinary Hall coefficient in amorphous FePC alloys is obtained above the Curie temperature, namely at 350°C. This value is $+3 \times 10^{-11}$ volt-cm/volt-cm/amp-G. An analysis of experimental data[55] on the electrical conductivity and the Hall coefficient for liquid metals and semiconductors indicates that the Hall coefficient and the carrier mobility generally decrease during the process of melting or when the long range order is destroyed. Busch and Tieche[56] measured Hall-effect of some metallic liquid elements (none of them ferromagnetic) over a wide temperature range and obtained a Hall coefficient very close to the calculated values and independent of temperature. They concluded that the electrical properties of liquid metals can be described on the basis of a free electron model. Bradley et al.[57] in their series of papers on electrical properties of liquid metals also indicate the validity of the nearly free electron approximation for liquid metals, i.e. $R_o = \left(\left(\frac{N}{V}\right) n^* e\right)^{-1}$ where $\left(\frac{N}{V}\right)$= number of atoms per unit volume, n^* = number of current carrier per atom.

If this formula is applied to the present results, it leads to a net approximate hole carrier density (holes minus electrons) of 0.01 hole/atom, assuming that N/V is equal to 0.085×10^{30} atoms/m^3. The temperature dependence of the Hall coefficient could not be measured because the maximum field obtainable with the magnet was not high enough.

In the case of ferromagnetic solids, the Hall electromotive force per unit current density ϵ_H can be expressed as

$$\epsilon_H = R_o B + R_s \times 4\pi M$$

in which B is the magnetic induction, M the magnetization in the solid and R_o and R_s are the ordinary and the spontaneous Hall coefficients. Since in the present experiments the magnetic field was perpendicular to the foil, the demagnetization field H_d is equal to $4\pi M$. The magnetic induction B is therefore

$$B = H + 4\pi M - H_d = H$$

and

$$\epsilon_H = R_o H + R_s 4\pi M$$

and

$$\frac{\partial \epsilon_H}{\partial H} = R_o + R_s \frac{\partial 4\pi M}{\partial H} \qquad (2)$$

The amorphous ferromagnetic foil has a coercive force of about 3 oersted.[11] The longitudinal magnetization curve (the hysteresis loop) is similar to that of soft iron type (curve 1, Fig. 27), and the transverse magnetization curve is shown in curve 2, Fig. 27. Therefore $\frac{\partial \epsilon_H}{\partial H}$ is equal to $R_o + R_s$ before the magnetization saturates and equal to R_o after the

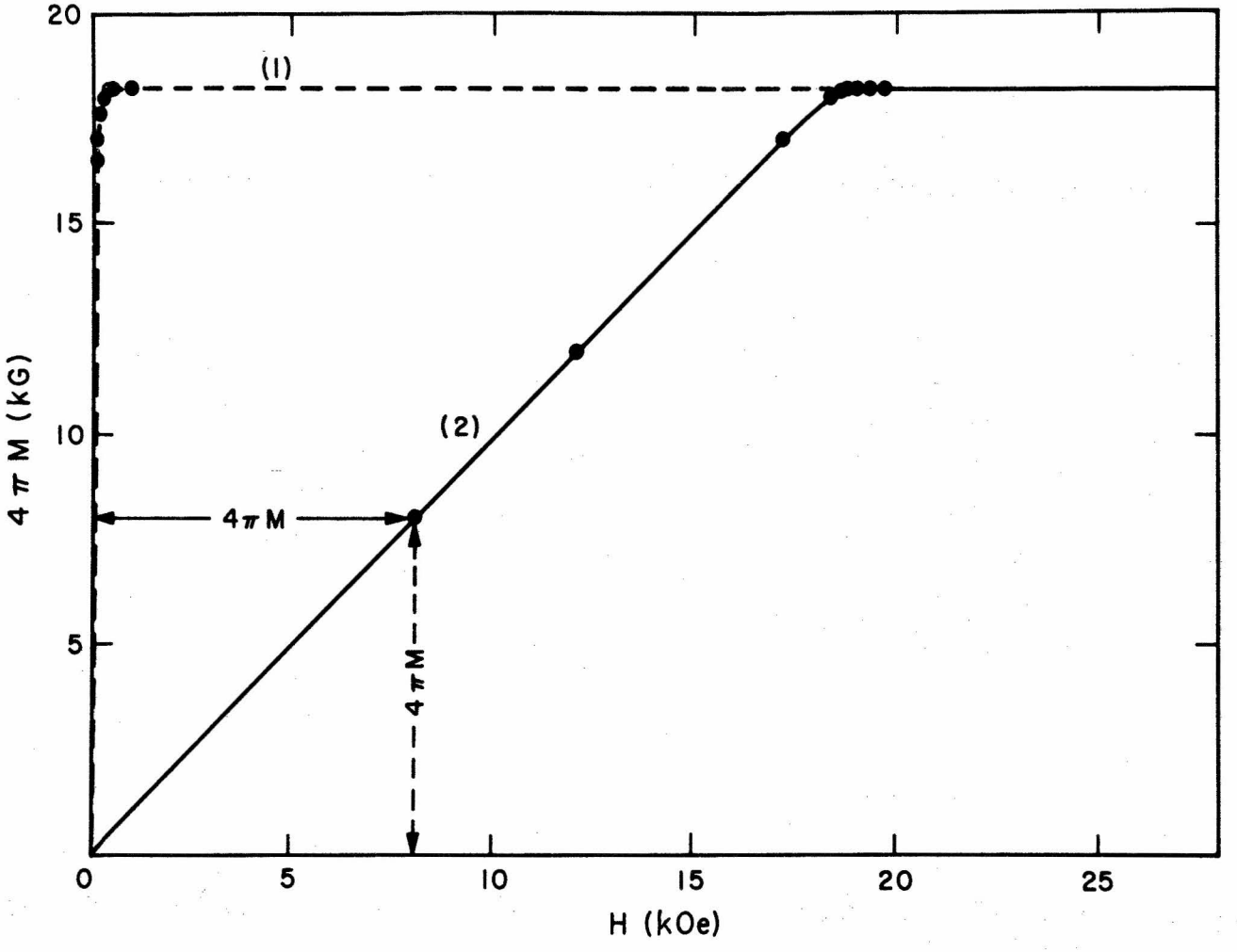

Fig. 27. Magnetization versus external magnetic field of amorphous FePC foil with magnetic field parallel (1) and perpendicular (2) to the foil surface.

magnetization saturates or when the temperature is larger than the Curie temperature.

The Hall electromotive force per unit current density has been measured with the maximum magnetic induction of 9.5 kG (Figs. 12,13). The ordinary Hall coefficient is not separable from the spontaneous Hall coefficient with magnetic field below 9.5 kG and at temperatures below room temperature. In most cases, the absolute values of R_o in ferromagnets do not differ by one order of magnitude from the corresponding values of the Hall constants of nonferromagnetic metals. For instance, Volkenshtein and Fedorou's[58] measurement at room temperature gives $R_o = + 0.20 \times 10^{-12}$ volt-cm/amp-G for pure iron and $R_o = -0.45 \times 10^{-12}$ volt-cm/amp-G for pure nickel, $R_o = -0.85 \times 10^{-12}$ volt-cm/amp-G for pure cobalt.

Two assumptions are necessary for the next derivation: 1) R_o in amorphous ferromagnetic FePC is smaller than R_s by at least one order of magnitude. 2) R_o does not vary significantly with temperature especially at low temperature. The second assumption is reasonable because in almost all liquid metals the ordinary Hall coefficient R_o is independent of temperature within the limits of error.[57]

From the results shown in Figs. 14 and 15, it may be concluded that in amorphous FePC, R_s is very large and almost temperature independent throughout the temperature range from $4.2^{o}K$ to $500^{o}K$. The value of R_s decreases by less than 1% from room temperature to liquid helium temperature. It should be noted that the sample which has the smaller temperature coefficient of electrical resistance also has the smaller temperature variation of R_s (Table II). It is probable that in an "ideal

amorphous" sample R_s would be independent of temperature.

The small temperature coefficient of the curve shown in Fig. 14 is about $20 \times 10^{-6}/C$ which is of the order of the volume coefficient of thermal expansion (e.g. iron has $35 \times 10^{-6}/^{o}C$). Therefore the temperature dependence of R_s is probably due to thermal expansion if R_o is independent of temperature.

As first noted by Rudnitskii,[59] the spontaneous Hall coefficient R_s may be related to the spin-orbit interaction of the current carriers. However no satisfactory explanation has been offered for the magnitude and the temperature dependence of the results obtained with crystalline specimens. In 1954, Karplus and Luttinger[60] showed that the interband matrix elements of the applied electric potential energy combined with the spin-orbit perturbation give a current perpendicular to both the field and magnetization. By taking into account the lattice periodicity, the calculated R_s was found strongly dependent on the temperature. These theoretical considerations gave a satisfactory explanation for the measurements made on iron, except in the low temperature region. Soffer, Dreesen and Pugh[61] proposed various explanations for the failure of the theory at low temperature but they could not reach definite conclusions. In addition, the theory did not explain the results obtained on nickel and cobalt. Before Karplus and Luttinger obtained their temperature dependency of R_s, Samoilovich and Kon'kov[62] used the following Hamiltonian,

$$H = \frac{P^2}{2m} + V(\vec{r}) + \frac{\mu_B}{2mc} (\vec{\sigma} \times \vec{E}) \cdot \vec{P} \qquad (1)$$

in which P is the momentum vector, $\vec{E}$ is the electric field in solid and is assumed spherically symmetric, $\vec{\sigma}$ is the Pauli matrix vector and μ_B is the Bohr-magneton. By assuming a nearly free electron wave function, they calculated the time variation of the electron density in momentum space as a result of the spin-orbit interaction, and without using the lattice periodicity condition, obtained a temperature independent coefficient.

Since in their calculations Samoilovich and Kon'Kov did not assume the existence of long range order (crystal lattice) their conclusions should be applicable to liquid metals and alloys as well as to amorphous alloys. The experimental results obtained in the present investigation gives strong support to their theoretical derivations. Thus the nearly free electron model explains not only the ordinary Hall coefficient in most liquid metals but also qualitatively predicts the temperature independence of the spontaneous Hall coefficient in amorphous ferromagnetic alloys.

The results of the magneto-resistance measurements described in section III.C.will now be discussed. The linear decrease in the tranverse magneto-resistance shown in Fig. 16 is characteristic of ferromagnetic metals.[63,64,65] The negative slope can be explained on the basis of a decrease in the scattering of electrons from 4s states to 3d states using the model of s-d scattering in ferromagnetic metals.[66] This decrease may be due to a reduction in the density of 3d states at the Fermi surface parallel to the field.

The positive contribution at room temperature is very small relative to the total resistance and could be due either to domain boundary scattering or to anisotropies introduced by changes in the relative direction of magnetization and current. Isin and Coleman[63] suggested that in pure iron the transverse magneto-resistance due to magnetic domain is positive at room temperature and exhibits maxima for field values in the range of 2 to 5 kOe. The fact that the FePC alloys are amorphous would not exclude these possibilities since magnetic domains have been found in this alloy,[67] and some evidence has also been found for a certain degree of anisotropy (see appendix IV).

In pure iron a rapid increase in resistance at high fields and low temperature is an expected behavior and results from the Lorentz force on the electrons when the mean free path is sufficiently long so that $\frac{eH}{mc} \tau = \omega_c \tau \geq 1$ (τ = relaxation time, ω_c = cyclotron frequency). In an amorphous solid, the relaxation time is short and the Lorentz term will need lower temperatures and higher fields to become important. This is the reason why the magneto-resistance in crystalline iron reaches the minimum at about 4 kOe and in amorphous iron the minimum may be far up between 10 and 20 kOe. At liquid helium temperature, amorphous sample starts to bend upward after 5 kOe; this may be the sign of the Lorentz term.

D. Curie Temperature and Spontaneous Magnetization

It is interesting to compare the Curie temperature of the amorphous FePC alloy, namely, 315°C with those of the ferromagnetic crystalline phases in Fe, Fe-P and Fe-C alloys. These temperatures are: 768°C for Fe, or Fe with maximum carbon in solution,[68] 420°C for Fe_3P; 80°C for Fe_2P and about 210°C for Fe_3C. The fact that the Curie temperature of the amorphous alloy is much lower than that of pure iron may be due to the difference in interatomic distances between iron-iron pairs which is 2.48A in iron and about 2.6A in the amorphous alloy. The distance 2.6A in the amorphous case is obviously an average, and it is probable that in this case the exchange interaction varies greatly between different pairs of atoms and consequently, the total exchange interaction might be greatly reduced. The effect of phosphorus on the Curie temperature is probably important. According to Haughton[69] the extrapolation of the α-phase Curie temperature to 25 atomic percent of phosphorus would be about 300°C. It is interesting to note that this temperature is not very far from that found for the amorphous alloy. A systematic study of the relationship between the Curie temperature and the composition of the alloy would probably yield interesting results. Since with the present state of development of the rapid cooling technique, an amorphous phase in FePC alloys can be obtained only within a rather narrow range of concentrations, such a study is not possible.

The spontaneous magnetization in FePC amorphous alloys may be deduced from the magnetic moment measurements. These measurements

showed that the moment of the iron atom in the amorphous alloy is $2.10\mu_B$ compared with $2.22\mu_B$ in pure iron. According to Gambino[70], the magnetic moments of the transition metals in their phosphides are always reduced. In Fe_3P, Fe_2P and FeP, these moments are 1.84, 1.32, and 0.36 respectively. In Fe_3C however, the moment is rather high and equal to $2.015\mu_B$. These reduced moments are assumed to be the result of the partial filling of the 3-d orbitals by electron transfer from phosphorus and carbon. The relatively high moment found for iron in the amorphous alloy is tentatively attributed to the high covalency between iron and either phosphorus and carbon atoms existing in the model proposed in section IV.B. for the structure of amorphous alloy $Fe_{80}P_{13}C_7$.

A study of the Mössbauer spectrum of amorphous FePC[71] has shown that it was not possible to explain the spectrum with models involving either a unique field or a continuous field. A reasonable fit was obtained with five fields of 175.4 ± 1.5, 213.8 ± 1.0, 244.3 ± 0.8, 270.8 ± 0.7 and 297.4 ± 1.6 kG. The weighting factors for each field were 0.144, 0.205, 0.245, 0.265, 0.144. The average magnetic hyperfine field varied with temperatures above $T/T_c \sim 0.65$ according to a Brillouin function with $J = 1$. The results obtained from the measurements of the bulk magnetization as a function of temperature agree with the hyperfine field variation between room temperature and liquid helium temperature. The $J = 1$ Brillouin function variation at high temperature should only be considered a coincidence and characterizes only an average over a distribution of magnetization weighted according to its probability.

Gubanov[72] has calculated the Curie temperature and magnetization as a function of temperature in an amorphous solid by assuming a radial distribution function for ferromagnetic atoms and an exchange integral which is only function of distances between two ferromagnetic atoms. If the Bethe's[73] curve of exchange interaction calibrated with pure iron exchange energy and together with the radial distribution function obtained from Chapter III are inserted in the Gubanov's calculation one obtains Tc $\approx 450^{o}$C which is not far from 315^{o}C by experiment. No meaningful results were obtained in applying Gubanov's theory to the calculation of the magnetization as a function of temperature. The reason for this failure may be due to the fact that the value of the exchange integral was not the correct one. In addition,Gubanov's model does not take into consideration the short range ordering which is present in amorphous FePC.

V. CONCLUSIONS

A detailed study has been made of the structure of an amorphous iron-phosphorus-carbon alloy obtained by rapid quenching from the liquid state. On the basis of the radial distribution function, the number of the nearest neighbors in the structure is seven at a distance of 2.6 Å. A model for the atomic arrangement in amorphous FePC is proposed. This model consists of a random network of trigonal prisms similar to those existing in the crystal structures of the compounds Fe_2P and Fe_3C in which the iron atoms have an average ligancy of seven. Such a network model is very similar to that generally accepted for the structure of fused silica, which is based on a random network of tetrahedra.

The electrical resistance of the amorphous alloy has a very low temperature coefficient (between 0.7×10^{-4} and $3.0 \times 10^{-4}/^{\circ}C$) and a high residual value at absolute zero (in the range of 90 to 98.4% of the room temperature resistance). This is explained by the fact that most of the scattering is due to the high degree of disorder in the structure and the contribution of the thermal scattering to the resistance is relatively small. A minimum in the resistance-temperature curve was observed in the range of 10° to $50^{\circ}K$. The exact reason for this minimum is not known at the present time. The temperature at which the minimum occurs, as well as the slope of the resistance-temperature curve at $300^{\circ}K$, and the residual resistance were found to vary from specimen to specimen. However, these three factors varied in a systematic way and it was concluded that the scatter in the

measurements made on several specimens were due to the presence of a small number of crystals in the amorphous matrix.

The ferromagnetic nature of the amorphous FePC alloy has been definitely established. The Curie temperature determined by both the induction method and Mössbauer spectroscopy is 315°C. The magnetic moment of the Fe atom in the amorphous alloy is 2.10 ± 0.01 Bohr magnetons per atom. The ordinary Hall coefficient is approximately 10^{-11} volt-cm/amp-G. The spontaneous Hall coefficient is about 0.6×10^{-9} volt-cm/amp-G. Experimental and theoretical studies of Hall coefficient in liquid metals have shown that it should be temperature independent. Since the spontaneous Hall coefficient of the amorphous alloy was found to be independent of temperature, this constitutes another proof that the structure of the alloy is indeed very closely related to that of the liquid state. The field dependence of the magneto-resistance at temperatures from liquid helium to room temperature is similar to that found in crystalline iron.

REFERENCES

1. S. Fujime, Japan J. Appl. Phys. 5 Number 11, 1029-35 (1966).
2. C. W. B. Grigson, D. B. Dove and G. R. Stilwell, Nature 204 173 (1964).
3. S. Mader and A. S. Nowick, App. Phys. Letter 7 Number 3, 57 (1965).
4. Pol Duwez and R. H. Willens, Trans. A.I.M.E. 227 362-365 (1962).
5. P. Pietrokowsky, Rev. Sci. Instr. 34 445-446 (1962).
6. W. Klement, Jr., R. H. Willens and Pol Duwez, Nature 187 809 (1960).
7. P. Predecki, B. C. Giessen and N. J. Grant, Trans. A.I.M.E. 233 1438-1439 (1965).
8. Pol Duwez, R. H. Willens and R. C. Crewdson, J. Appl. Phys. 36 2267-2269 (1965).
9. R. C. Crewdson, Ph.D. Thesis, California Institute of Technology (1966).
10. Huey-Lin Luo, Ph.D. Thesis, California Institute of Technology (1964).
11. Pol Duwez and S. C. H. Lin, J. Appli. Phys. 38 4096 (1967).
12. Martin E. Weiner, Ph.D. Thesis, California Institute of Technology (1968).
13. B. D. Cullity, Elements of X-ray Diffraction, p. 106 (Addison-Wesley Publishing Company, Inc.) (1959).
14. D. T. Cromer, Acta Cryst. 18 17 (1965).
15. D. T. Cromer and J. T. Waber, Acta Cryst. 18 104 (1965).
16. B. E. Warren, H. Krutter and O. Morningstar, J. Am. Ceram. Soc. 19 202 (1936).
17. C. J. Pings and J. Washer, Private communication.
18. J. Washer and V. Schomaker, Rev. of Mod. Phys. 25 No. 3, 671 (1953).
19. H. Ruppersberg and H. J. Seeman, Z. Naturforschg. 21a, 820-826 (1966).

20. S. Fujime, Japan, J. Appl. Phys. 5 1029 (1966).

21. R. W. Powell, Phil. Mag. 44 772 (1953).

22. N. P. Mokrovskoi and A. R. Regel, Zhurnal Tekhnicheskei Fiziki (Moskow) 23 2121 (1953).

23. H. S. Chen and D. Turnbull, Appl. Phys. Letters 10 No. 10, 284 (1967) andTechnical Report No. 13, Division of Engineering and Applied Physics, Harvard Univ. Cambridge, Mass.

24. G. Hagg, J. Chem. Phys. 3 42 (1935).

25. A. I. Gubanov, Quantum Electron Theory of Amorphous Conductions, p. 70 (Consultant Bureau, 1965).

26. J. Frenkel, "Properties of Liquids and Mechanism of Fusion", Kinetic Theory of Liquids, Clearendon Press, Oxford (1946).

27. S. Fujime, Japan, J. Appl. Phys. 5 778 (1966).

28. S. Fujime, Japan, J. Appl. Phys. 5 643 (1966).

29. S. Fujime, Japan, J. Appl. Phys. 5 739 (1966).

30. Siegfried Steeb,Zeitschrift für Metallkunde, Band 57 Heft 2, 97-103 (1966).

31. R. C. Buschert, Ph.D. Thesis, Purdue University (1957).

32. Gerhard Breitling, 2nd Conference on the Characterization of Materials, Rochester, New York (1967).

33. S. Fujime, Japan, J. Appl. Phys. 5 764 (1966).

34. Richter and S. Steeb,Nature 51 512 (1958).

35. J. Kakinoki, K. Katada, T. Hanawa and T. Ino, Acta Cryst. 13 171 (1960).

36. B. L. Averbach, Second Conference on the Characterization of Materials, Rochester, New York (1967).

37. W. H. Zachariasen, J. Am. Chem. Soc. 54 3841 (1932).

38. P. Debye and H. Menke, Erg. Techn. Rontgenkunde 2 1 (1931).

39. W. E. Morrell, J. H. Hildebrand, J. Chem. Phys. 4 224 (1936).

40. W. W. Wood and F. R. Parker, J. Chem. Phys. 27 720 (1957).

41. J. D. Bernal, Nature 185 68 (1960).

42. J. K. Percus and C. J. Yevick, Phys. Rev. 110 (1958) and Phys. Rev. Letters 8 462 (1962).

43. A. A. Broyles, S. U. Chung and H. L. Sahlin, J. Chem. Phys. 37 2462 (1962).

44. H. S. Green, The Molecular Theory of Fluids, Interscience Publishers Inc., New York (1952).

45. S. E. Rodriquez, C. J. Pings, J. Chem. Phys. 42 No. 7, 2435-2437 (1965).

46. M. H. Cohen and D. Turnbull, Nature 203 964 (1964).

47. Stig Rundqvist, Acta Chemica Scandinavica 16 1-19, (1962).

48. Stig Rundqvist, and Franz Jellinek, Acta Chemica Scandinavica 13 425-432 (1959).

49. H. Lipson and N. J. Petch, The Journal of Iron, Steel Instit. Vol. CXLII, No. 2, 95 (1940).

50. L. Pauling, The Nature of Chemical Bond, p.421 3rd Ed. Cornell University Press, Ithaca, New York (1960).

51. L. Pauling, The Nature of Chemical Bond. p. 93-99, 3rd Ed. Cornell University Press, Ithaca, New York (1960).

52. R. L. Myuller, The Structure of Glass, Vol. 2, p. 50, Proceedings of the Third All-Union Conference on the Glassy State, Leningrad, November, 1959, published by Consultant Bureau, New York (1960), translated from Russian.

53. G. J. van den Berg, Proceedings of the 7th International Conference on Low Temperature Physics (ed. G. M. Graham and A. C. Hollis-Hallett. University of Toronto Press,1961) and G. J. van den Berg and J. de Nobel, J. Phys. radium 23 665 (1962).

54. Jun Kondo, Progress of Theor. Phys. 32 No. 1, 37 (1964).

55. A. R. Regel, Ukrains'kyi Fizychnyi Zhurnal 7 833 (1962).

56. G. Busch and Y. Tieche, Compte rendu de la réunion de la Société Suisse de Physique 35 273 (1962).

57. C. C. Bradley, T. E. Faber, E. G. Wilson and J. M. Ziman, Phil. Mag. 7 868 (1962).

58. N. Y. Volkenshtein and G. V. Fedorou, Soviet Phys. J.E.T.P. 11 48 ; J. Exptl. Theoret. Phys. (U.S.S.R.) 38 64-68 (1960).

59. V. E. Rudnitskii, J.E.T.P. 9 262 (1939).

60. R. Karplus and J. M. Luttinger, Phys. Rev. 95 1154 (1954).

61. S. Soffer, J. A. Dreesen and E. M. Pugh, Phys. Rev. 140A 668 (1965).

62. A. Samoilovich and U. Kon'kov, J. Exptl. Theoret. Phys. (U.S.S.R.) 20 782 (1950).

63. Acar Isin and R. V. Coleman, Phys. Rev. 142 372 (1966).

64. Velio A. Marsocci, Phys. Rev. 137A 1842 (1965).

65. J. Smit, Physica 17 612 (1951).

66. N. F. Mott, Advan. Phys. 13 325 (1964).

67. Pol Duwez, Transactions of the Am. Soc. of Metals 60 No. 4, p. 630 (1967).

68. M. Hansen, Constitution of Binary Alloys (1958).

69. J. L. Haughton, J. Iron Steel Inst. 115 417 (1927).

70. R. J. Gambino, McGuire and Nakamura, J. Appl. Phys. 38 1253 (1967).

71. C. C. Tsuei, G. Longworth and S. C. H. Lin, to be published in Phys. Rev.

72. A. I. Gubanov, Soviet Phys-Solid State 2 468 (1960).

73. H. Bethe, Handb. d. Physik 24 pt. 2, 595-8.

APPENDIX I

Phase Diagrams of Fe-P and Fe-P-C

The phase diagram of iron-phosphorus is well documented and is reproduced in Fig. A-1 taken from Ref. 1. The dotted lines on this diagram corresponds to metastable states. A metastable eutectic exists at 945^{o}C between Fe and Fe_2P. This diagram can be obtained by slow cooling and the Fe_3P phase in this case is suppressed.

The phase relationships in the ternary Fe-P-C system have not been accurately established, and the only available data are shown in Fig. A2 (taken from Ref. 2). The ternary eutectic temperature is given as 953^{o}C, but the eutectic composition is not exactly known. However, the $Fe_{80}P_{13}C_7$ alloy studied in the present investigation is probably not far from the eutectic composition.

---

1. M. Hansen, Constitution of Binary Alloys, p. 693, McGraw-Hill Book Co. Inc. New York (1958).

2. C. H. Desch, Correspondence to Stead's paper, J. Iron Steel Inst. 91 195 (1915).

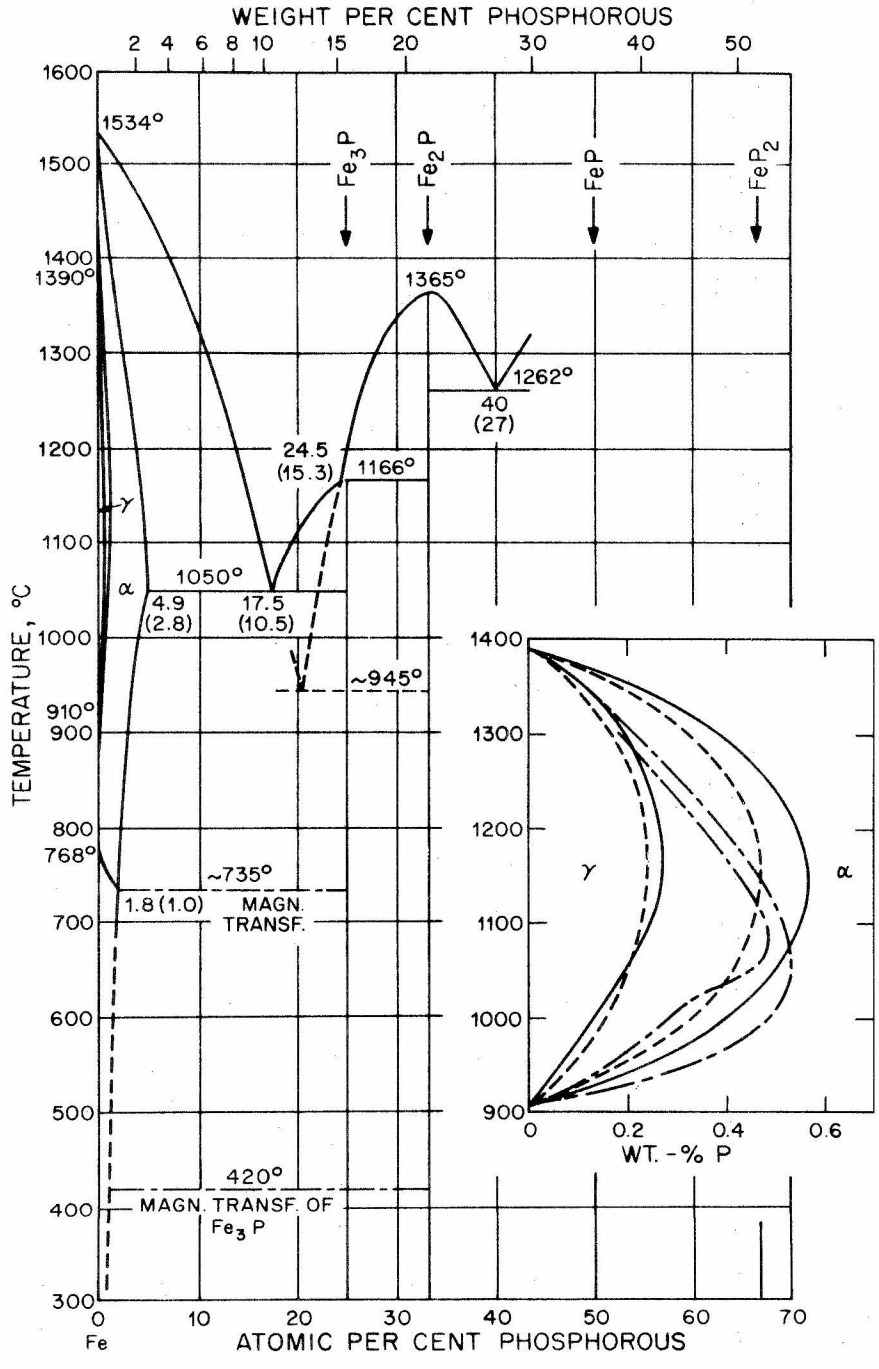

Fig. A-1. Fe-P binary phase diagram

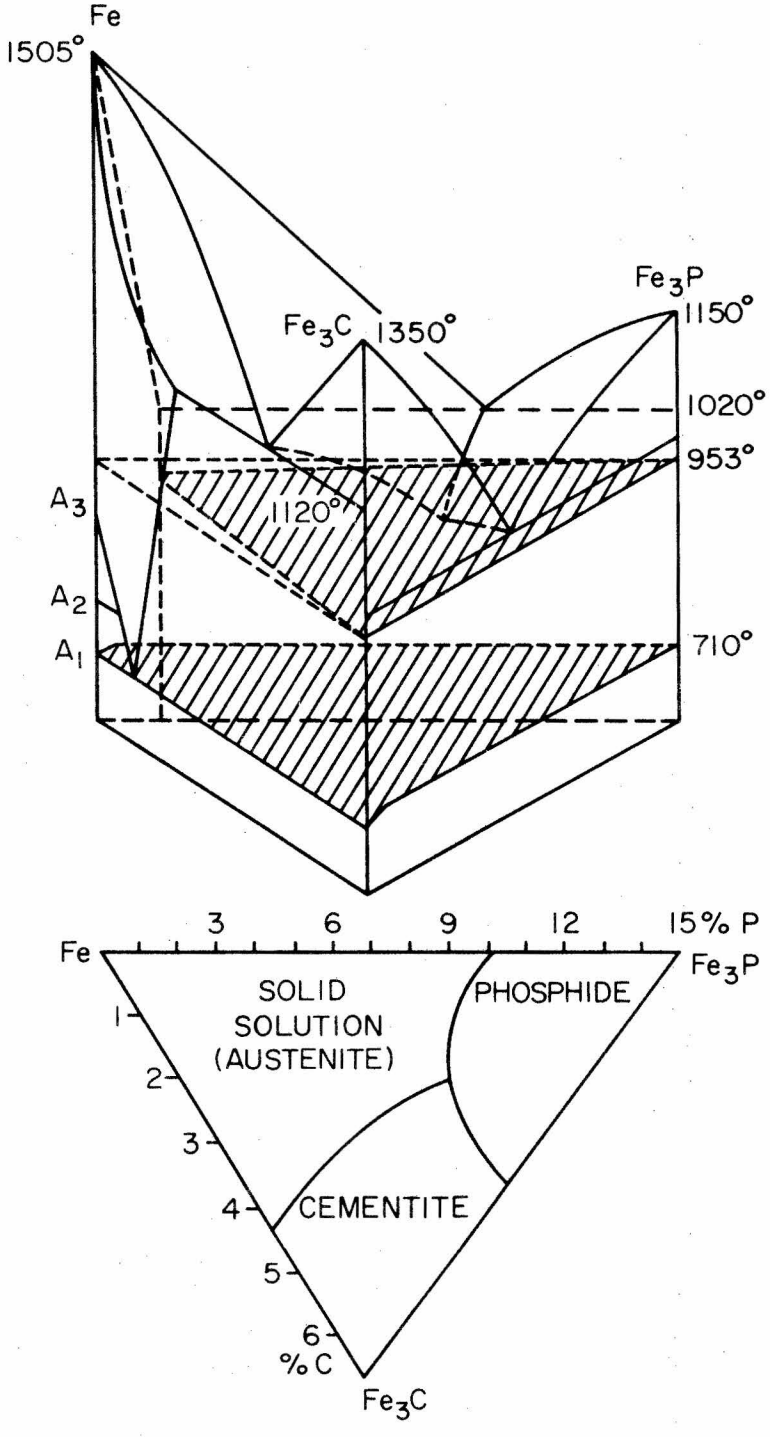

Fig. A-2. Fe-P-C ternary phase diagram

APPENDIX II

Densities of Amorphous and Crystalline Fe-P-C Alloys

The densities of both amorphous and crystalline FePC alloys were determined by the picnometer method in connection with a microbalance and using pure acetone (density 0.792 gr/cm^3). The measurements were repeated on several specimens and the average values so obtained are compared with the densities of pure iron (taken from Ref. 1) in the following table:

Materials	Density (gm/cm^3)
Amorphous FePC	6.97 $\pm$ 0.05
Crystalline FePC	7.223 $\pm$ 0.002
α-Fe	7.873 (20°C)
γ-Fe	7.646 (916°C)
δ-Fe	7.356 (1394°C)

---

1. Barrett & Massalski, Structure of Metals, McGraw-Hill (1966) p. 628.

APPENDIX III

Radial Distribution Calculation of Fe-Fe Correlation in Fe_3P, Fe_2P and Randomnized α-Fe Lattices

Rundqvist's Fe_3P crystal structure[1] and Rundqvist and Jellinek's F_2P crystal structure[2] were used for this calculation. The unit cell of Fe_3P contains 24 Fe atoms and that of Fe_2P contains 6 Fe atoms. Starting from a given Fe atom around the center of the model the distances between this atom taken as origin and all the other Fe atoms in the 250 unit cells were calculated. This operation was repeated 24 times for Fe_3P and 18 (3 x 6) times for Fe_2P. The number of atoms located at distances between r and r + Δr, in which Δr = 0.2Å, was then calculated. The radial distribution function of Fe-Fe correlation obtained by this method were shown in Fig. 25.

Models for the liquid state have been obtained by starting from the crystal structure of the element and displacing the atoms from their equilibrium position in a random fashion. This method was used as early as 1930 by Debye and Menke,[3] who calculated the radial distribution function of liquid mercury, starting from its hexagonal crystal structure. Since the number of neighbors in amorphous FePC is seven, body centered alpha iron was chosen as a starting point. The model consisted of hard

---

1. Stig Rundqvist, Acta Chemica Scandinavica 16 11, (1962).
2. Stig Rundqvist, Franz Jellinek, Acta Chemica Scandinavica 13 425 (1959).
3. P. Debye and H. Menke, Physik Z. 31 797 (1930).

spheres representing iron atoms with a radius of 0.75 Å (that of Fe^{2+} according to Pauling). A total of 15x15x15 unit cells,(a total of 6750 atoms) were considered and every atom was displaced along three orthogonal axes. The extent of these displacements was limited by the maximum distance available until contact occurred between spheres. The numerical values of these displacements were obtained from a computer subprogram producing random numbers. The radial distribution function was calculated as explained above for Fe_3P and Fe_2P, and is shown in Fig. 25.

APPENDIX IV

The Magnetic Anisotropy

The magnetic anisotropy of amorphous FePC was measured with circular samples of 1.35 cm diameter and about 50μ thick. An automatic torque balance developed by Humphrey and Johnston[1] was used and the magnetic field was applied parallel to the surface of the foil. A maximum field of only 4 oersted (due to the limitation of maximum acceptable torque of the instrument) was applied and was enough to show some anistropy in the amorphous alloy. The anisotropic constant was calculated to be approximately 3.2 dyne-cm/c.c. for 4 Oe. applied field (Coersive force 3 Oe.). The existence of the anisotropy in an amorphous phase has been considered as an indication of possible submicroscopic heterogeneity[2] in some inorganic glasses.[3,4] The anisotropy which may be the consequence of high strain during the rapid quenching should eventually vanish for "ideal amorphous" samples defined in section III.B.

---

1. F. B. Humphrey, A. R. Johnston, Jet Propulsion Lab. Technical Report No. 32-321 (1962).

2. W. A. Weyl, E. C. Marboe, Fundamentals of the Structure of Inorganic Liquids and Solids.

3. P. W. Selwood, Magnetochemistry, Ed. 2, InterScience, New York (1956) p. 189.

4. K. Banerjee, J. Am. Ceram. Soc. 36 296 (1953).